DI Sara Kurakin, BSc

Integration and Application of Optical Carbon Dioxide Sensors in Microbioreactors

MASTER'S THESIS

to achieve the universitiy degree of

Diplom-Ingenieurin (Dipl.-Ing.)

Master's degree programme: Technical Chemistry

submitted to

Graz University of Technology

Supervisor

Assoc.Prof. Dipl.-Chem. Dr.rer.nat. Torsten Mayr

Institute of Analytical Chemistry and Food Chemistry

Graz, February 2019

EIDESSTATTLICHE ERKLÄRUNG

Ich erkläre an Eides statt, dass ich die vorliegende Arbeit selbstständig verfasst, andere als die angegebenen Quellen/Hilfsmittel nicht benutzt, und die den benutzten Quellen wörtlich und inhaltlich entnommenen Stellen als solche kenntlich gemacht habe. Das in TUGRAZonline hochgeladene Textdokument ist mit der vorliegenden

Masterarbeit identisch.

…… ……

Datum Unterschrift

AFFIDAVIT

I declare that I have authored this thesis independently, that I have not used other than the declared sources/resources, and that I have explicitly indicated all material which has been quoted either literally or by content from the sources used. The text document uploaded to TUGRAZonline is identical to the present master‘s

thesis dissertation.

…… ……

Date Signature

Abstract

CO_2 is an important analyte and quantification of CO_2 is of great interest e.g.: in medicine, food industry, environmental monitoring as well as in biotechnology for process monitoring. Measurement of CO_2 as well as O_2 and pH is an important factor for bioprocess control. For that fluorescence based optical sensors show several advantages over conventional methods, such as reduced noise, no consumption of the analyte and minimal invasive measurements. This is especially necessary for small scale systems and for fermentations in microbioreactors.

During the last decades different optical CO_2 sensors had been developed. Beside several advantages of optical sensors, the main drawbacks are interferences with acidic gases and limited stability. Further challenges of CO_2 sensors occur due to sensitivity to osmotic pressure, limited shelf life and long response times.

In this study an optical CO_2 sensor was developed and together with an O_2 and pH sensor it was integrated into a microbioreactor. Cultivations of *S. cerevisiae* and *S. carnosus* were investigated using these sensors and OD_{600} measurements. The designed sensor was based on monoOH azaBODIPY dye, which shows good photostability, small drifts, low risk of leaching and little sensitivity to changes in ionic strength.

The sensors were successfully integrated into the microbioreactor and CO_2 was measured in gas and liquid phase. The response times were below one minute and measurement up to 25 % CO_2 was possible, with high sensitivity at low CO_2 concentrations. The sensors showed reasonable stability for the application in a microbioreactor. Measurements were possible at RT as well as at 37 °C and the sensors were insensitive to changes of the reaction media. Cultivation of *S. cerevisiae* and *S. carnosus* in the microbioreactor and online monitoring of CO_2 production, O_2 consumption, cell growth and pH was achieved. Cultivations of *S. carnosus* showed a CO_2 production up to 10 % with a final OD_{600} of 20 and minimum pH of 6. A maximum CO_2 concentration of 2.5 % with a final OD_{600} of around 0.7 and increasing pH over the fermentation time was detected during fermentation of *S. cerevisiae*.

Zusammenfassung

CO_2 ist ein wichtiger Analyt und dessen Quantifizierung in den Bereichen der Medizin, Lebensmittelindustrie, Umweltanalytik sowie Prozesskontrolle in der Biotechnologie ist von großer Bedeutung ist. Besonders in der Bioprozesskontrolle ist neben CO_2 auch die Bestimmung von O_2 und pH-Wert ein wesentlicher Faktor. Für diesen Zweck zeigen Fluoreszenz-basierte optische Sensoren einige Vorteile gegenüber herkömmlichen Analysemethoden. Zu diesen zählen verringertes Rauschen, wenig invasive Messungen sowie kein Verbrauch des Analyten, was vor allem im kleinen Maßstab und bei Kultivierung im Mikrobioreaktor wichtig ist.

In den letzen Jahrzehnten wurden verschiedene optische CO_2 Sensoren entwickelt. Trotz der Vorteile von optischen Sensoren zeigen diese auch einige Nachteile, wie begrenzte Stabilität und Wechselwirkungen mit sauren Gasen. Die Verwendung von optischen CO_2 Sensoren kann zu weiteren Limitierungen, wie geringe Lebensdauer, lange Ansprechzeiten und Empfindlichkeit gegenüber osmotischem Druck, führen.

In dieser Arbeit wurde ein optischer CO_2 Sensor entwickelt und gemeinsam mit pH und O_2 Sensoren in einen Mikrobioreaktor integriert. Diese Parameter sowie die optische Dichte wurden während Fermentationen von *S. carnosus* und *S. cerevisiae* überwacht. Der Farbstoff monoOH azaBODIPY wurde für den entwickelnden Sensor verwendet, auf Grund seiner guten Eigenschaften bezüglich Fotostabilität und Driftverhalten sowie geringem Risiko von Ausblutung und wenig Sensitivität gegenüber Änderung der Ionenstärke.

Nach erfolgreicher Integration der Sensoren, konnte CO_2 sowohl in der Flüssig-, als auch in der Gasphase gemessen werden. Ansprechzeiten unter einer Minute wurden bestimmt und Messungen bis zu 25 % CO_2 waren möglich, wobei die höchste Sensitivität bei niedrigen Konzentrationen erzielt wurde. Für die Anwendung zeigten die Sensoren ausreichende Stabilität. Messungen konnten sowohl bei RT als auch bei 37 °C durchgeführt werden und waren weitgehend unabhängig vom Reaktionsmedium. *S. cerevisiae* und *S. carnosus* konnten im Mikrobioreaktor, mit erfolgreicher online Analyse der CO_2 Produktion, des O_2 Konsums, Zellwachstum sowie pH, kultiviert werden. Während der Kultivierung von *S. carnosus* wurde eine maximale CO_2 Konzentration von 10 %, eine finale OD_{600} von 20 und ein minameler pH von 6 gemessen. Die Kultivierung von *S. cerevisiae* erzielte eine maximale CO_2 Konzentration von 2,5 %, bei einer finalen OD_{600} von 0,7 mit stetig steigendem pH Wert.

Danksagung

Als erstes möchte ich mich bei Assoc. Prof. Torsten Mayr für die Möglichkeit bedanken auf diesem tollen Institut meine Masterarbeit schreiben zu können. Danke für die Unterstützung und Gelegenheit, mein Wissen im Bereich der Chemosensoren erweitern zu können, sowie für die Chance einen Teil der Arbeit an der TU Braunschweig zu absolvieren.

Ein großes Dankeschön geht auch an Prof. Rainer Krull, der es mir ermöglichte an der TU Braunschweig den Bereich der Microbioreaktorten zu erkunden. Dieser Forschungsaufenthalt hat mich nicht nur fachlich sondern auch persönlich weitergebracht.

Ein riesiges Danke natürlich auch an die beiden tollen Arbeitsgruppen in denen ich meine Masterarbeit machen durfte. Ohne euch als Kollegen wäre diese Zeit nicht annähernd so lustig gewesen.
Mein besonderer Dank geht dabei an David (als mein inoffizieller Betreuer), sowie Philipp und Berni für die Unterstützung bei der Entwicklung der Sensoren. Liebe SexySensors danke für die tolle Zeit, die Kaffeepausen und Feierabendbiere!

Danke auch an Lasse für die Unterstützung bei den Mikrobioreaktoren. Und Hendrik: Vielen Dank für deine Hilfe im Labor und mit deinen Reaktoren und dass du meine Launen ertragen hast wenn nicht alles nach Plan lief. Ohne dich wären die Versuche nicht so gut gelaufen.

Vielen Dank auch an Marie, für den Ausflug nach Hamburg und die vielen tollen Stunden in Brauschweig.

Ein großes Danke geht natürlich an meine Eltern: für die finanzielle als auch moralische Unterstützung bei all meinen Entscheidungen. Vielen Dank, dass ihr mir auch ein zweites Masterstudium ermöglicht habt. Ohne euch wäre ich nie so weit gekommen.

Anna, ich bin stolz dich als große Schwester zu haben, danke, dass du immer für mich da bist auch wenn wir jetzt schon lange nicht mehr zusammen in Graz wohnen. Und Tobi, danke, dass ich mit dir bei einem Gläschen Wein (oder so) noch manchmal vergessen kann, dass meine Studienzeit beinahe vorbei ist.

Lieber Christian, danke für deine Unterstützung und Liebe. Ich bin froh mit dir zusammen zu leben, auch wenn wir gelegentlich im Chaos versinken. Vielen Dank, dass ich immer auf dich zählen kann!

Einen herzlichen Dank möchte ich auch an Silvia und Sarah aussprechen. Es war immer eine geile Zeit mit euch und ohne euch hätte das Studieren keinen Spaß gemacht. Die wohlverdienten Feierabende in Gleisdorf nach ‚erfolgreichem' Lernen werde ich nie vergessen.

Magdalena, natürlich auch dir ein riesiges Danke. Danke, dass du immer da bist, für die jahrelange Freundschaft, dafür dass wir über alles reden können und für die ‚Mittwochs-Dates', die nicht nur das kulinarische Highlight der Woche sind.

Content

1 Introduction 1

1.1 Luminescence - Principles 1

1.2 Characteristics of fluorescence 3

1.3 Luminescence - measurement techniques 8

1.4 Chemosensors – Definitions and principles 12

1.5 Optical sensors for bioprocess control 14

1.6 CO_2 - sensing 15

1.7 pH and O_2 sensing 20

1.8 Microbioreactor systems 22

1.9 Integration of sensors in microbioreactors 25

2 Materials and Methods 27

2.1 Materials 27

2.2 Methods – sensor preparation 29

2.3 Methods – sensor characterization and analytics 34

2.4 Methods – sensor application in microbioreactor 36

3 Results and discussion 45

3.1 Sensor development and preliminary characterization 45

3.1.1 Investigation of the CO_2 sensor composition 45

3.1.2 Measurements in gas and liquid phase 47

3.1.3 Influences of temperature on measurements 49

3.1.4 Response time measurements 49

3.2 Characterization of CO_2 sensor spots 51

3.2.1 Sensor stability 51

3.2.2 Sensitivity 56

3.2.3 Reproducibility 57

3.2.4 Dependence on reaction media 59

3.3 Application of O_2, CO_2 and pH sensors in microbioreactor 60

3.3.1 Reactor design and application 60

3.3.2 Cultivation of S. carnosus 61

3.3.3 Cultivation of S. cerevisiae 64

4 Conclusion 66

5 Abbreviations 67

6 Literature 68

7 Tables and Figures 73

8 Appendix 78

1 Introduction

1.1 Luminescence - Principles

Luminescence is described as the emission of light from an electronically excited state. There exist several types of luminescence, where fluorescence and phosphorescence are two particular cases thereof. Absorption of photons generates a species in an electronically excited state, while de-excitation occurs through photon emission. Depending on the nature of the excited state, this occurs by fluorescence or phosphorescence. [1a][2a]

After absorption of a photon, emission through fluorescence is one possibility; however, there are also other possible pathways. The Jablonski diagram (Figure 1) shows a few of these pathways.

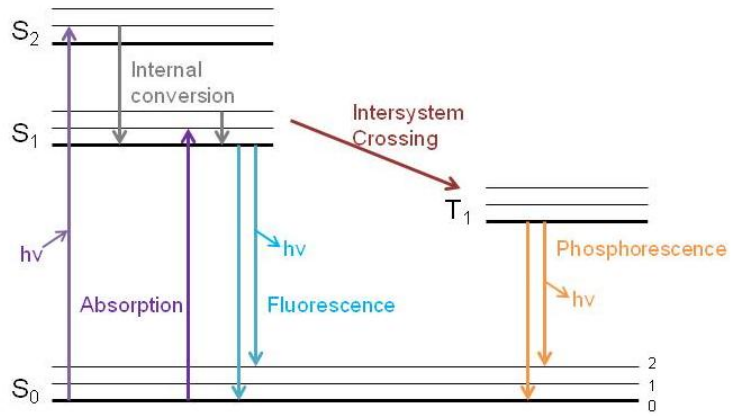

Figure 1: Jablonski diagram – one schematic form. S_0, S_1 and S_2: singlets in ground, first and second electronic state. T_1: first triplet state. 0, 1 and 2 indicate the vibrational energy levels of each state. [2a]

Absorption usually occurs from the ground state S_0, exhibiting the lowest vibrational energy. So the fluorophore is excited to the first or second state and mainly to a higher vibrational energy level. At this point usually relaxation to the lowest vibrational energy of S_1 occurs, called internal conversion. Internal conversion is with around 10^{-12} s much faster than fluorescence emission (~10^{-8} s) and hence completed prior to emission. Fluorescence emission occurs from the lowest vibrational level of S_1 usually to an excited vibrational level of the ground state. [2a]

From S_1 also spin conversion to T_1 could occur, called intersystem crossing. The emission from the first triplet state is called phosphorescence. Actually, transition from T_1 to S_0 is

forbidden and hence emission times are several orders of magnitude larger compared to fluorescence. [2a]

1.2 Characteristics of fluorescence

1.2.1 Fluorescence quenching

Quenching means a decrease in fluorescence intensity and can happen due to several processes. One of these mechanisms is collisional (dynamic) quenching, where deactivation of the excited molecule occurs through collision with a quencher. Many molecules can act as quencher, such as oxygen, amines or halogens.

$$\frac{F_0}{F} = 1 + K_{SV}[Q] = 1 + \mathrm{k_q}\tau_0[\mathrm{Q}] \qquad \text{equ.1}$$

F_0/F ... fluorescence intensity (initial/quenched)

K_{SV} ... Stern-Volmer constant [$L.mol^{-1}$]

[Q] ... concentration of the quencher [$mol.L^{-1}$]

k_q ... bimolecular quenching constant [$mol.L^{-1}.s^{-1}$]

τ_0 ... unquenched lifetime [s]

The Stern-Volmer equation (equ. 1) describes this decrease in intensity, where the Stern-Volmer constant also includes the accessibility and sensitivity of the fluorophore to the quencher.

Besides collisional quenching, it can occur via other mechanisms, such as formation of non-fluorescent complexes at the ground state (static quenching). [2a]

1.2.2 Photoinduced electron transfer – PET

PET is a further possibility for fluorescence quenching. In this process an electron donor (D) and an electron acceptor (A) molecule form a complex.

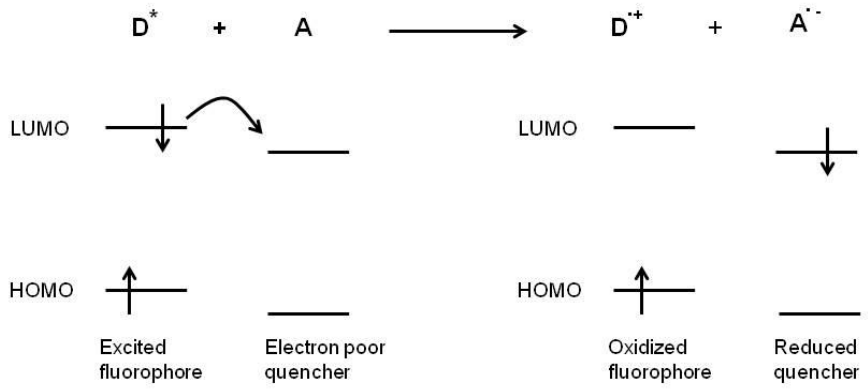

Figure 2: Scheme for oxidized electron transfer using PET. [1b]

There are two possibilities of electron transfer: reductive and oxidative (as shown in Figure 2; equ. 2).

$$A^* + D \rightarrow A^{\bullet-} + D^{\bullet+} \qquad \text{equ.2}$$
$$D^* + A \rightarrow D^{\bullet+} + A^{\bullet-}$$

It might happen that the formed complex returns to the ground state without photon emission, but it is also possible that exciplex emission occurs. Finally, the transferred electron returns from the acceptor to the donor. The terms donor and acceptor only define the electron transfer and not the species which is initially in the excited state. [1b][2b] In this study the used dyes for the pH sensor as well as the CO_2 sensor rely on the principle of PET. [3][4]

1.2.3 Stokes shift

Usually, fluorescence emission exhibits less energy than the corresponding previous absorption. So fluorescence emission typically occurs at higher wavelengths. The difference between the maximum of the first absorption and fluorescence emission is called Stokes shift. It can provide important information about the exited state. This energy loss is commonly caused by fast relaxation from a higher excited state to the lowest vibrational level of S_1. Generally, the detection of fluorescence is easier when the Stokes shift is larger. [1c][2a]

1.2.4 Quantum yield and lifetime

Fluorescence lifetime and quantum yield are two essential factors for characterization of fluorophores. Equation 3 and 4 describe the quantum yield and lifetime.

$$Q = \frac{\Gamma}{\Gamma + k_{nr}} \qquad \text{equ.3}$$

$$\tau = \frac{1}{\Gamma + k_{nr}} \qquad \text{equ.4}$$

Q ... quantum yield

τ ... fluorescence lifetime [s]

Γ ... emission rate of the fluorophores [s^{-1}]

k_{nr} ... rate of non-radiative decay [s^{-1}]

The quantum yield describes the ratio between absorbed photons and those which return to the ground state through photon emission. Beside photon emission, non-radiative decay can occur (e.g. through internal conversion).

The fluorescence lifetime is given as an average time where the fluorophore remains in the exited state. The fluorescence lifetime is usually around 10 ns. Lifetime as well as quantum yields are dependent on many parameters such as temperature, pH, viscosity or presence of a quencher such as oxygen. Quantum yields should be high since this facilitates observation of fluorescence. [1d][2a]

1.2.5 Emission and excitation spectra

Generally spoken, the fluorescence or emission spectrum is independent of the excitation wavelength. It can be assumed that emission takes place from the lowest vibrational state of S_1 and energy from higher vibrational levels is fast dissipated by internal conversion. However, there are also exceptions e.g.: if there exist two or more ionization states of a fluorophore and some molecules also emit from the S_2 level. [1e][2a]

The emission spectrum is characteristic for each molecule and it shows the emission from the lowest energy level of S_1 to any vibrational state of S_0. Concerning the emission spectrum, also the fluorescence intensity should be regarded. It can be expressed as written in equ. 5.

$$I_F(\lambda_F\lambda_E) = kF_\lambda(\lambda_F)I_A(\lambda_E) \qquad \text{equ.5}$$

I_F ... fluorescence intensity

F_λ ... emission spectrum

k ... proportionality factor

I_A ... intensity of absorbed photons

λ_E ... excitation wavelength [nm]

λ_F ... wavelength for measuring fluorescence [nm]

So, the intensity of fluorescence is proportional to the emission spectra, recorded at a certain wavelength, and the intensity of absorbed photons. The proportionality factor depends on certain variables such as the optical configuration of the measuring instrument and the band width of the used monochromator.

$$I_A(\lambda_E) = I_0(\lambda_E) - I_T(\lambda_E) \quad \text{equ.6}$$

$$I_T(\lambda_E) = I_0(\lambda_E)e^{-\varepsilon cl} \quad \text{equ.7}$$

I_0 ... intensity of incident light

I_T ... intensity of transmitted light

ε ... molar absorption coefficient [$L.mol^{-1}.cm^{-1}$]

c ... concentration [$mol.L^{-1}$]

l ... optical path [cm]

The intensity of absorbed photons can be expressed as given in equ. 6 and the intensity of transmitted light is defined by the law of Lambert-Beer (equ. 7). Thus fluorescence intensity is only proportional to the concentration in diluted solutions. At high fluorophore concentrations the inner filter effect causes decrease in fluorescence intensity. Some photons might be re-absorbed due to an overlap of absorption and emission spectra and thus reduce the intensity. [1e]

1.2.6 Resonance energy transfer – RET

Resonance energy transfer describes the process of a non radiative energy transfer between a donor and an acceptor molecule. This process occurs in the excited state and requires an overlap of the emission band of the donor with the absorption band of the acceptor (Figure 3). Here no photons are transferred but electronic energy of the donor. This is usually caused by dipole-dipole interaction between donor and acceptor. [1f][2c]

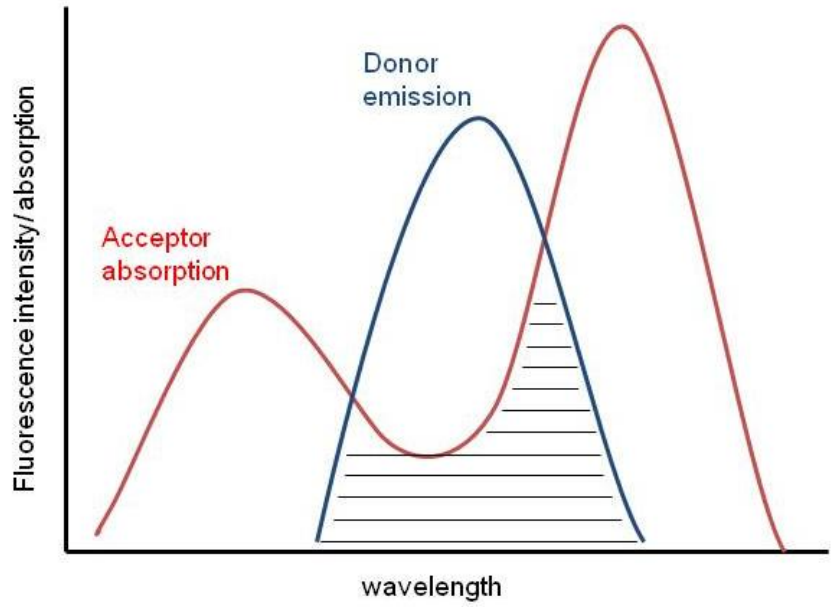

Figure 3: RET – spectral overlap of absorption and emission spectrum. [2c]

The extent of energy transfer depends on the distance between donor and acceptor as well as on the spectral overlap. The rate of energy transfer was described by Föster according to equ. 8.

$$k_T(r) = \frac{1}{\tau_D}\left(\frac{R_0}{r}\right)^6 \qquad \text{equ.8}$$

k_T ... energy transfer rate [s^{-1}]

r ... distance between donor and acceptor [m]

R_0 ... Föster distance [m]

τ_D ... lifetime of donor without energy transfer [s]

The Föster distance defines the critical distance between donor and acceptor, where probability of energy transfer and decay of the excited donor is the same. Hence, the energy transfer depends on the distance between these molecules, where Föster distances are usually in the range between 30 and 60 Å. [1f][2c]

1.3 Luminescence - measurement techniques

Spectrophotometers for measurement of fluorescence require a broad range of optical instruments, where the main parts include:

- a light guide, such as optical fibres or planar waveguide-based sensor platforms
- a light source, where e.g. LEDs, arc or incandescent lamps or lasers might be used
- a monochromator
- a photodetector
- an amplifier and read out [2d][5]

Fluorescence sensors can be intrinsic or extrinsic. In the first case the analyte itself is fluorescent and might be directly measured (e.g.: NADH). More often, the analyte has no fluorescent properties (e.g.: when measuring CO_2, pH or oxygen). In this case an indicator molecule is used, which changes its optical properties upon reaction or interaction with the analyte. [6][7a]

1.3.1 Fibre optical chemical sensors – FOCS

Optical fibres are widely used for optical chemosensors. In principle there are passive and active FOCS, where active FOCS are modified in a way that they change their optical properties due to interaction with the analyte. Several configurations can be used, including cladded or doped fibres or fibre bundles. Measurements of absorption as well as fluorescence are possible.

In a simple set-up, one fibre is used for measuring fluorescence. The excitation wavelength is first delivered through the fibre to the sensor and then the emitted light is collected and transported to an appropriate detector. [6]

1.3.2 Measurement of lifetime and intensity

Measurements of fluorescence can be done based on either intensity or lifetime. Regarding the instrumental set-up, intensity measurements are simpler, however, suffer from several drawbacks. Changes of the light source, photobleaching or differences in the indicator concentration can cause drifts of the signal. For that reason lifetime measurements are favoured, since they are insensitive to those parameters.

Lifetime measurements again can be divided in two different types. On the one hand lifetime itself (time domain) can be measured, one the other hand lifetime can be determined via phase modulation techniques (frequency domain).

In time-domain lifetime measurements, a light pulse is applied to the fluorescent probe for excitation. The pulse is as short as possible and has to be much shorter than the lifetime of the fluorophore. Time dependent intensity can be measured with this method and thus the lifetime is calculated. This method often requires complex and costly instrumentation such as intensified CCD cameras or photon counting photomultiplier tubes.

For that reason development of frequency domain measurements was enforced. Here the excitation light source is modulated at a certain frequency. The intensity of incident light is usually modulated at frequencies near 100 MHz, so that the reciprocal frequency can be compared to the reciprocal lifetime. Excitation of the fluorophore with modulated frequency causes the emission to respond in the same way. The emission is delayed in time compared to the excitation due to the lifetime of the fluorophore. This is measured as a phase shift, which can be used to calculate decay times (equ. 9).

$$tan\phi = 2\pi f\tau \qquad \text{equ.9}$$

Φ ... phase angle [°]

f ... frequency of modulation [Hz]

τ ... lifetime [s]

The measured phase shift depends on the modulation frequency and the lifetime and also the peak height of the emission decreases relative to modulated excitation. The measured phase angle increases and the modulation of the emission decreases with increasing frequency. [2e][6]

The fluorescence lifetime of the indicator molecule has to be in the microsecond range to allow modulation with appropriate frequencies for application of a frequency domain measurement. This is possible for oxygen sensors based on ruthenium or porphyrin complexes, however, in case of e.g.: CO_2 and pH sensors, lifetimes of the indicators are too short. Hence, various strategies were developed to render intrinsically intensity based methods applicable for phase modulation measurements. One of these methods is dual lifetime referencing (DLR). [6]

1.3.3 Dual lifetime referencing

DLR is used for lifetime based measurements to overcome drawbacks of intensity measurements. It can be used for frequency and time-domain measurements. For that the indicator dye, which has a short lifetime, is coupled with a reference dye having a long lifetime. [6][8][9]

In the frequency domain, the phase shift of the overall fluorescence is measured, which depends only on the ratio of indicator- and reference luminescence.

A

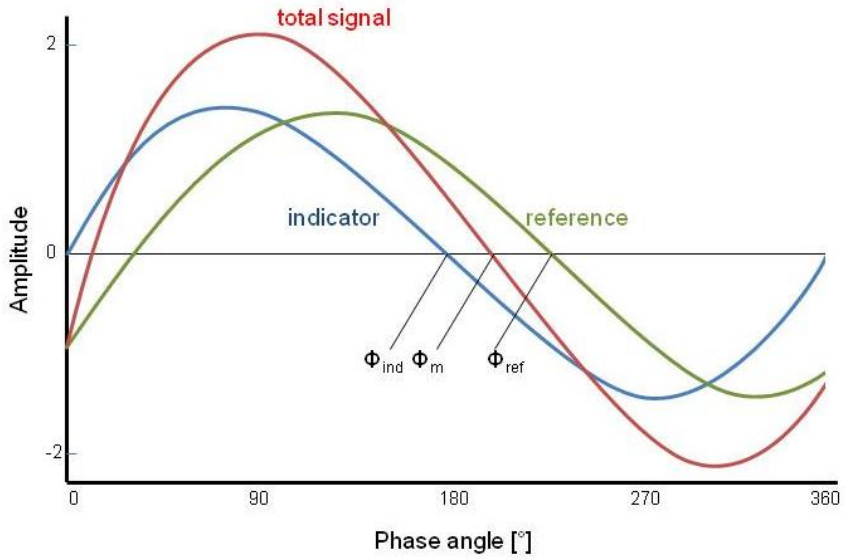

B

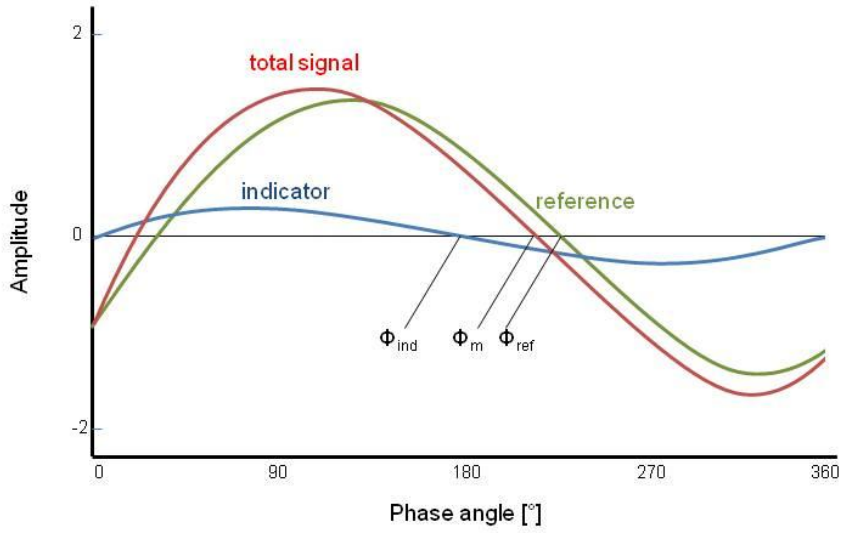

Figure 4: Scheme of DLR. A: In absence of the analyte the indicator is in its unquenched state. B: Presence of the analyte which quenches the fluorescence signal of the indicator. The overall phase angle changes. [8]

Figure 4 shows a scheme of DLR in presence and absence of the analyte. The reference dye remains unaffected by the analyte, while presence of the analyte quenches the indicator dye resulting in changes of the amplitude. The intensity of the indicator dye is reflected by the phase angle of the reference and thus related to the analyte concentration. The used modulation frequency is only based on the reference dye with the long lifetime. [6][8]

1.4 Chemosensors – Definitions and principles

According to IUPAC, a chemosensor is defined as follows: "*A chemical sensor is a device that transforms chemical information, ranging from the concentration of a specific sample component to total composition analysis, into an analytically useful signal. The chemical information, mentioned above, may originate from a chemical reaction of the analyte or from a physical property of the system investigated."* (IUPAC 1991, [10]) A chemical sensor needs to consist of at least a receptor and a transducer. The receptor is able to react with the analyte providing the chemical information in a form of energy that can be measured by the transducer. The transducer then converts this chemical information into an analytically useful signal. [10][11a][12a]

1.4.1 Classification

There are various possible classifications for chemosensors, where a common way is classification according to the transducer. Following sensor types might be distinguished: [10]

- Optical sensors, which are based on changes in the optical properties due to interaction of the sensor with the analyte. The optical properties might be based on absorbance, reflectance, luminescence, light scattering, optothermal effects or refractive index.
- Electrochemical sensors, related to electrochemical interaction between analyte and electrode.
- Electrical sensors, where changes of electrical properties occur, but without electrochemical reactions.
- Mass sensitive sensors, based on the mass change of a surface due to accumulation of the analyte.
- Magnetic sensors, measuring differences in paramagnetic properties.
- Thermometric sensors, related to heat effects caused by a chemical reaction or adsorption of the analyte.

Further classification might be done based on the measured analyte (e.g.: O_2 sensors) or the mode of application (e.g.: in-vivo). [10]

In this study a fluorescence based CO_2 sensor was used. Hence in the following chapters, the principles of optical fluorescence sensors and CO_2 sensing will be described.

1.4.2 Performance factors and requirements for an ideal sensor

For a good performance of a chemical sensor there are a few important parameters to consider. The most important factor is the selectivity, where ideally the sensor only responds to the desired analyte. Further, it should have a good sensitivity and accuracy, fast response and recovery times. Moreover, it is desired that the sensor is small, inexpensive and easy to calibrate. Furthermore, also reversibility, a high stability and low sensor drift are important factors. Other factors regarding the long-term stability, limit of detection and dynamic range mainly depend on the desired application. [12b][13]

A chemical sensor should be able to continuously measure a certain analyte. Measurements can be performed at-line, on-line or off-line, while in this study the sensors where integrated into the microbioreactor (MBR) and therefore online measurement of CO_2, O_2 and pH was done. The main advantages of online measurements are real time analysis and process control at process temperature, without the need of sampling, disrupting the production flow or high risk of contamination. However, there are some disadvantages such as possible interaction of the sensor with the reactants, increase in the complexity of the system, the need of regular re-calibration or replacement of the sensor, limitation to a specific problem and difficult quantification of cross-sensitivity. [13]

1.5 Optical sensors for bioprocess control

In the past decades, genetic engineering and study of recombinant organisms for production of proteins as therapeutics and their use in industry increased rapidly. Hence also methods for accurate process control became more important. [14] Following parameters should be recorded for monitoring of a fermentation culture: CO_2, O_2, pH and often nutrients such as glucose. [14] One method would be the use of fluorescence based optical sensors. Sensors that are used in fermentation cultures should be sterilizable (e.g. with EtOH or gamma-radiation) and show little drift, e.g. due to variations in ionic strength and temperature of the medium. Further, background and noise, due to scattering or adsorption of light by the medium, should be minimized and fouling of the sensor has to be avoided. [14]

Fluorescence based sensors have several advantages over other analysis methods for bioprocess control. Optical effects, e.g. related to product formation, substrate binding or analyte concentration might be measured due to interaction of the fluorescent dye with light. Since no electromagnetic interferences occur with light, noise can be reduced by the use of optical sensors. Other than electrochemical or enzymatic methods, fluorescence sensors do not consume or transform the analyte upon measurements. Measurements usually take place when equilibrium between analyte and indicator dye is reached. This is especially important when measuring at very low analyte concentrations. Moreover, detection of photons is possible without a direct contact of sensor and sample. Excitation and detection could be performed from outside, e.g. through a transparent wall, while the fluorescence sensor is placed in the fermentation broth. This enables minimal invasive measurement compared to electrochemical sensors, where a direct contact is necessary for detection of the electrons. [14]

However, there are also some drawbacks when using fluorescence sensors in biotechnological processes. The noise ratio usually increases due to miniaturization, since fluorescence signals vary with scale. Mostly, the relationship of analyte concentration and output signal is non-linear which lowers the dynamic range of the sensors compared to electrochemical ones. Often also the costs are limiting since complex optics and electronics are needed to generate excitation light and for detection. [14]

1.6 CO_2 - sensing

1.6.1 Why measure CO_2

CO_2 is an important analyte and measurement of CO_2 is of great interest e.g.: in medicine, food industry and environmental monitoring such as for maritime analysis. [11b][15][16][17][18] Further, measuring of the CO_2 concentration is also an important task in biotechnology for process monitoring, since microbial growth can be greatly influenced by CO_2. [18][19][20]

1.6.2 Behaviour of CO_2 in liquid medium

CO_2 dissolves weakly in aqueous phase. Dissolved CO_2 reacts to carbonic acid, which can further dissociate to HCO_3^- and CO_3^{2-}(equation 10 – 13). Solubility and equilibrium are strongly affected by the pH. [20][21a][22a][23a]

$CO_2\ (g) \leftrightarrow CO_2\ (aq)$	$K_1 = 3.3*10^{-2}\ mol.L^{-1}.atm^{-1}$	equ.10
$CO_2\ (aq) + H_2O \leftrightarrow H_2CO_3$	$K_2 = 2.6*10^{-3}\ mol.L^{-1}.atm^{-1}$	equ.11
$H_2CO_3 + H_2O \leftrightarrow HCO_3^- + H_3O^+$	$K_3 = 1.72*10^{-4}\ mol.L^{-1}$	equ.12
$HCO_3^- + H_2O \leftrightarrow CO_3^{2-} + H_3O$	$K_4 = 5.59*10^{-11}\ mol.L^{-1}$	equ.13

According to Henry's law (equ 14) the solubility of CO_2 in the solution can be calculated (equ 15). However, since CO_2 (aq) is in equilibrium with H_2CO_3 according to equ. 10 – 13, the calculated value in pure water is the sum of CO_2 and H_2CO_3.

$$x_A = \frac{P_A}{H} \qquad \text{equ.14}$$

x_A ... mole solute analyte/mole solution

P_A ... partial pressure of A [atm]

H ... Henry's law constant [$atm^{-1}.mol_{analyte}^{-1}.mol_{solution}^{-1}$]

$$c_{CO2} = \frac{P_{CO2}}{H} \qquad \text{equ.15}$$

cCO_2 ... concentration CO_2 [mmol/L]

pCO_2 ... partial pressure of CO_2 [atm]

H ... Henry's law constant [$L.atm^{-1}.mmol^{-1}$]

1.6.3 CO_2 sensors

There are two main types of optical CO_2 sensors used, which rely both on the principle of measuring pH changes in dependence of the CO_2 concentration. An optical pH sensor is therefore incorporated into a gas permeable matrix. The earlier type was an optical sensor developed according to the Severinghaus electrode, and later the more commonly used plastic- or Mills type sensor was designed. [15][17][20][24a][25][26]

Further, also IR measurements are used for CO_2 sensing. These sensors are robust; however, they can only be applied in the gas phase. Moreover, they are expensive and water vapour strongly affects the measurement. [16][17][18]

1.6.4 Severinghaus electrode and sensors

The Severinghaus electrode was first developed for measuring CO_2 in blood. It is based on pH measurement of a very thin film of bicarbonate solution. This bicarbonate solution is in equilibrium with the CO_2 amount in the unknown sample. A CO_2 permeable Teflon membrane, which is impermeable for ions, is used to prevent interferences between sample pH and measured pH in the electrode. As pH electrode, a glass electrode was used with silver as reference. Sodium bicarbonate with NaCl was used as electrolyte, which was soaked into cellophane. The cellophane was placed in between the Teflon and the glass electrode to provide a reinforced waterfilm. [27] CO_2 diffuses through the membrane and changes the pH depending on pCO_2. Main drawbacks of the Severinghaus electrode are its bulkiness and its relatively long response time. Further, it is quite expensive and could be affected by other acidic gases or by changes in osmotic pressure. [20]

The pCO_2, depending on the equilibrium of CO_2 (equ. 10 – 13), can be calculated as given by equ. 16. [20]

$$\alpha * p_{CO2} = [H_2CO_3] = \frac{[H^+]^3 + [H^+]^2[Na^+] - K_W[H^+]}{K_3([H^+] + 2K_4)} \qquad \text{equ.16}$$

$\alpha = K_1K_2[H_2O]$

K_W ... water dissociation constant

However, equ. 16 can be simplified (equ. 17) if an excess of sodium bicarbonate is used.

$$\alpha * p_{CO2} = [H_2CO_3] \approx \frac{[H^+][Na^+]}{K_3} \quad \text{equ.17}$$

The early developed optical CO_2 sensors used the same principle as the Severinghaus electrode. The so called 'covered wet sensors' used a fluorescent pH sensitive dye (DH) instead of a pH electrode. The dye is dissolved in the bicarbonate solution and covered with a gas permeable membrane. According to the equilibrium (equ. 10 – 13), the dye is protonated or deprotonated, depending on its acid dissociation constant K_a (equ. 18 and 19), where the protonated and deprotonated form of the dye have very different emission and absorption properties. [20]

$$D^- + CO_2 + H_2O \leftrightarrow DH + HCO_3^- \quad \text{equ.18}$$

$$\alpha * p_{CO2} = [H_2CO_3] \approx \frac{K_a[HD][Na^+]}{K_3[D^-]} \quad \text{equ.19}$$

In the same way also a 'solid droplet sensor' was developed, where an emulsion of the dye and sodium bicarbonate solution was entrapped in a silicone matrix. However, the main drawback of those sensors is the sensitivity to vapour and osmotic pressure, and hence its limitation to systems with low changes in osmotic pressure. [20] Further, it has a limited shelf life as well as long response and recovery times. [25]

1.6.5 Solid state CO_2 sensors

Due to various drawbacks of the wet covered CO_2 sensors, a solid state or Mills type CO_2 sensor was developed. [15]

These sensors are based on a dry concept, where the bicarbonate buffer is replaced by a phase transfer agent (mainly a quaternary ammonium base, Q^+OH^-) and instead of the gas-permeable membrane a hydrophobic polymer is used. Often also a plasticiser is added to the mixture to enhance diffusion of CO_2 through the polymer and hence improve response times. The base is used for solubilising the indicator dye in the hydrophobic medium due to formation of an ion pair (Q^+D^-). Further, it provides an alkaline environment, which is necessary for CO_2 measurement and it allows inclusion of moisture into the polymer. The presence of water is still crucial for the measurement of CO_2 based on the pH and it is

assumed that a few molecules of water are associated with the ion pair ($Q^+D^-nH_2O$). Hence the overall process can be described by equ. 20. [13][15][20][24a][25]

$$\{Q^+D^-nH_2O\} + CO_2 \leftrightarrow \{Q^+HCO_3^-(1\text{-}n)H_2O\} + HD \qquad \text{equ.20}$$

Main advantages of this sensor type compared to the Severinghaus type are improved response times, less sensitivity towards osmotic pressure and long shelf life. [20] However, problems of limited stability due to irreversible reactions of the dye with acidic gases remain. [13][20]

1.6.6 Mono-OH azaBODIPY for CO_2 sensing

In this study a CO_2 sensor was designed based on monoOH azaBODIPY dye (Figure 5).

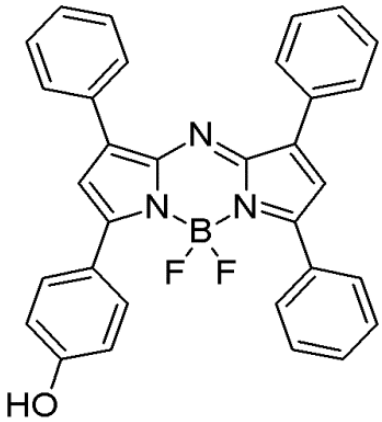

Figure 5: MonoOH azaBODIPY for optical CO_2 sensing.

This dye was reported by Jokic *et al.* as a fluorescent pH sensitive dye. AzaBODIPYs are of great interest for pH sensing due to the possibility of structural modifications and excellent photochemical properties. Usually they contain amino or hydroxy functional groups. Quenching of the fluorescence of the deprotonated form is caused by photoinduced electron transfer from the functional group to the azaBODIPY moiety. For pH sensing there are several reasons that favour an unsymmetrical form of the azaBODIPY, containing only one functional group. One the one hand there is a simple acid-base equilibrium, since there are only two forms of the dye and on the other hand these molecules are more hydrophobic, which lowers the risk of leaking. Further, due to the low charge it is expected to be less influenced by ionic strength. [3]

The following properties were determined for the dye (Table 1).

Table 1: Properties of monoOH azaBODIPY for pH sensing. [3]

Solvent	$\lambda_{abs\text{-}acid}$/ $\lambda_{abs\text{-}base}$ [nm]	$\lambda_{em\text{-}acid}$ [nm]	QY	ε [$M^{-1}cm^{-1}$]	pK_{abs}	pK_{em}
EtOH:H_2O	670/726	702	0.11		8.35	8.38
Hydrogel D4	687/742	718			8.47	8.09
THF			0.15	84000		

The designed pH sensor showed a good photostability, a small drift, is suitable for referencing methods and it is compatible with Firesting from Pyroscience (λ_{exc} = 620 nm). [3]

Despite the promising results regarding pH sensing, the asymmetric dyes were so far not used for CO_2 sensors. Schutting *et al.* used the di-OH azaBODIPY for CO_2 sensing since they found that with the unsymmetric forms the formed ion pair between the hydroxy group and the tetraoctylammonium hydroxide (TOAH) was very strong and hence prevented re-protonation of the sensor. [18] However, in this study $CsHCO_3$ was used as base instead of TOAH.

1.7 pH and O_2 sensing

1.7.1 Oxygen sensors

Optical oxygen sensors are based on the ability of oxygen to dynamically quench the fluorescence of fluorophores, which have a fluorescence lifetime higher than 10 ns. For the production of the sensor, usually a phosphorescent is immobilized in a host polymer. Often metal-ligand complexes with fluorescence lifetime of around 100 ns, such as Ru(II) bipyridine complexes or platinum or palladium porphyrin complexes, are used as phosphorescent dye. The sensitivity of the sensors can be influenced by the choice of the polymer and phosphorescent, since it is dependent on oxygen permeability, diffusion rate into the matrix and phosphorescent lifetime. For oxygen measurements usually the decay of fluorescent lifetime or intensity is recorded. The Stern-Volmer equation (equ. 21) can be used for description of the fluorescence quenching and as possibility for linearization of oxygen measurements. [11b][13][14]

$$\frac{\tau_0}{\tau} = \frac{I_0}{I} = 1 + K_{SV}[O_2] \qquad \text{equ.21}$$

I/I_0 ... luminescence intensity in presence/absence of oxygen

τ/τ_0 ... luminescence decay time in presence/absence of oxygen

K_{SV} ... Stern-Volmer constant [$L.mol^{-1}$]

$[O_2]$ ... oxygen concentration (quencher) [$mol.L^{-1}$]

1.7.2 pH sensing

Optical pH sensors are based on acid-base indicators, which change absorbance or fluorescence based on protonation and deprotonation. [11b][13][14]

Here two different types of fluorescence dyes can be distinguished: dual excitation indicators and emission ratiometric indicators. The first variant is similar to absorption based dyes. The protonated and deprotonated forms have different absorption maxima and extinction coefficients, but might have the same emission maxima. However, quantum yield is also dependent on excitation wavelength and hence emission intensities can be measured at two excitation wavelengths and the pH is determined based on their ratio. In the second type also the emission maxima is different and so the ratio of emission intensities can be used for determination of pH. [14]

Calibration of pH sensors typically shows an S-shaped curve, which can be fitted via the Boltzmann equation. The measurement range is usually limited to 1.5 units above and below the pK_a. Usually this is enough for biotechnological applications; however, the range can be broadened by combining pH indicators with different pK_a values. [11b][13][14]

Typical indicators are hydroxypyrene trisulfonic acid (HTPS), seminaphthorhodafluors (SNARF) or azaBODIPYs, which show enhanced photostability and are less dependent on ionic strength, compared to SNARFs and HTPS. [11b][13][14]

1.8 Microbioreactor systems

Screening of cell cultures and optimization of bioprocess conditions requires reproducible high-throughput technologies and efficient control of basic bioprocess parameter. The use of conventional fermenters is time consuming and expensive for this purpose, especially when testing high-cost substrates. For that reason, the demand for small systems enabling online process monitoring and hence the development of microbioreactors (MBRs), with reaction volumes below 1 mL, is enforced. Further advantages of MBRs are improved heat and mass transfer by increased surface to volume ratio and shorter distances for diffusion. [28][29]

However, there are several challenges in the design of MBRs. Due to the small volume the Reynolds number (equ. 22) decreases far below 1300 and thus MBRs work under laminar flow conditions in contrast to the turbulent conditions in conventional reactors. [28][29]

$$Re = \frac{\rho * \nu * L}{\mu} \qquad \text{equ.22}$$

μ ... viscosity of the fluid [$kg.m^{-1}.s^{-1}$]

ν ... fluid velocity [$m^3.s^{-1}$]

ρ ... density of the fluid [$g.m^{-3}$]

L ... characteristic length of the system [m]

Thus mixing is limited to molecular phenomena such as diffusion, which might cause dead zones and sedimentation of cells. Further problems might be caused by evaporation, leakage of media or interactions between materials and reactor. Moreover, the design should allow integration of sensors for online process monitoring. [28][29]

Cultivation might be done in microtiter plates, with volumes down to 25 µL, and there is also the possibility of sensor integration. However, it suffers from poor aeration rates and high risk of cross contamination at high shaking rates, while mixing is limited if the shaking rate is decreased. [30] Szita *et al.* reported a microbioreactor with a total volume of 5 µL including a sensor system. The reactor was based on PDMS allowing aeration of the culture. Although this is a promising set-up for screening, analysis is mainly limited to online techniques. [30][31]

Magnetic elements, peristaltic mixers or pumps are used for homogenous MBRs (hMBR). However, in such systems gas bubbles due to aeration or formation of CO_2 have to be avoided, since they have a negative effect on mixing. Furthermore, generated gas bubbles

could influence the stable laminar flow and cause clogging of the microchannels. Therefore, only passive oxygen supply through membranes is used and further formation of gas is decreased by use of degassed medium, increased pressure in the reactor or application of vacuum from outside. [28]

Another possibility is a micro bubble reactor which is analogous to bubble column reactors in large scale. Here the MBR is arranged in a vertical position and actively gassed through micronozzles. Mixing and oxygen supply is achieved by sparging with air, where homogenous distribution of cells and nutrients is dependent on the aeration rate. Additional advantages compared to the hMBR are the simple and cheap construction and low operation costs. [28]

PMMA or PDMS is often used for fabrication of the MBRs. These materials are cheap, easy in handling, biocompatible and resistant to many chemicals and solvents. Moreover, they are transparent for visible light which enables combination with optical measurement systems. [29] Fabrication techniques include soft-lithography, which is very common for PDMS, thin film deposition, wet- and dry etching as well as 3D-printing and laser micromatching. [32]

1.8.1 Oxygen uptake in cell cultures

Oxygen uptake is a critical parameter for cultivation of aerobic microorgansims. The required amount of oxygen input is defined by the oxygen consumption rate of the culture (equ. 23).

$$Q_O = q_O x \qquad \text{equ.23}$$

x ... cell concentration [$g.L^{-1}$]

q_O ... specific oxygen uptake [$mol.g^{-1}.s^{-1}$]

Q_O ... oxygen uptake rate [$mol.L^{-1}.s^{-1}$]

Since the solubility of oxygen is less than 10 ppm in aqueous media at ambient conditions, oxygen transfer into the media has to be fast. Oxygen transfer can be described by equ. 24.

$$N_A = k_L a(C^*_{AL} - C_{AL}) \quad \text{equ.24}$$

N_A ... oxygen transfer rate [mol.m^{-3}.s^{-1}]

k_L ... mass transfer coefficient in liquid phase [m.s^{-1}]

a ... gas-liquid interfacial area [m².m^{-3}]

C^*_{AL} ... oxygen concentration in equilibrium [mol.m^{-3}]

C_{AL} ... oxygen concentration in the media [mol.m^{-3}]

The oxygen transfer from the gas bubbles to the cells is influenced by many mass transport steps, where the rate limiting step of oxygen transfer is the transport through the liquid film surrounding the gas bubble. This is described by the k_La as shown in equ. 24. Combining equ. 23 and equ. 24, the oxygen transfer and consumption can be described for the steady state (equ. 25).

$$q_O x = k_L a(C^*_{AL} - C_{AL}) \quad \text{equ.25}$$

Improvement of the oxygen uptake in cell cultures can be achieved by various factors, which either improve the k_La or the driving force (C^*_{AL} - C_{AL}). The characteristics of the gas bubbles strongly influence the k_La, where their size is the most important factor. Smaller bubble sizes are preferred due to greater interfacial area and a diameter between 2 and 3 mm is considered as ideal. Bubble size and k_La are also influenced by media viscosity, where an increased viscosity decreases the oxygen uptake. Further, an increased stirrer speed or gas flow rate also improves the k_La. Additionally also the way how gas bubbles are formed, the effectiveness of gas dispersion or the addition of antifoam agents influence the oxygen transfer rate. Besides the k_La, also the solubility of oxygen can be influenced mainly by temperature and pressure, as described by Henry's law (see chapter 1.6.2, equ. 14). [33a]

1.9 Integration of sensors in microbioreactors

The possibility of sensor integration is an important feature for online measurements and analysis of fermentation cultures in MBRs. Sampling and offline measurements are usually not possible due to the low reaction volume. Often fluorescence based sensors are integrated into the MBRs (mainly made of PMMA or PDMS) for process control. [29]

There are several techniques which enable integration of fluorescence sensors into the MBR system.

The easiest way is dissolving the indicator in the medium and pumping it into the reactor together with the reagents. Although this results in immediate response, drawbacks are the presence of the dye in the product stream or possible interactions of dye and reactants. [13]

Therefore, a stationary sensor is preferred, where the dye is embedded in a polymer matrix, which is permeable for the analyte. For that usually sensor layers or spots are used, where analytes might be detected at different positions of the MBR channel. There are several approaches for the integration of stationary sensors. The methods often require a structuring step (such as cutting out a sensor spot) and gluing it into the MBR. Integration is the less challenging the bigger the channels and the smaller the spots are. Difficulties can occur due to overgrowing of the spots by adherent cells. Further, the signal intensity, stability and morphology of the sensor might be strongly influenced by the used methods. [13]

Following methods can be used for production of stationary sensor layers:

- direct staining of the MBR material

Here the sensor dye is directly embedded into the MBR material, e.g. using PDMS and mixing it with curing reagents and the dye. Difficulties might occur due to low permeability of the material or challenges in read out.

- Spin and knife coating

These techniques enable production of a sensor film with a thin layer. Spin coating is done in the following way: The sensor cocktail is put onto a smooth surface and spun to produce a film of a few hundred nanometres due to rotational forces. Structuring can be achieved through laser treatment. Knife coating is done at polymer foils or glass substrates, where a

'knife' with a defined gap to the surface is used. The sensor cocktail is spread with the knife and afterwards structuring can be achieved by cutting and gluing it into the MBR.

- Screen-printing

Here a mesh is prepared, which defines size and shape of the sensor and is coated with a blocking stencil, which is impermeable to the cocktail. The cocktail then can be put through the mesh onto the surface. Sensor spots down to 100 µm can be produced, but it is limited to planar surfaces.

- Photopolymerization

Very small sensor spots can be produced using this method. The photoresit matrix contains the sensor dye and can be cured with UV light. A photomask is used to cover the matrix and only expose those parts to the UV that represent the desired sensor area.

- Spray coating

A sensor cocktail is dissolved into an appropriate solvent and then sprayed onto a substrate. Here larger areas can be homogenously coated, also including pattering through masks or stencils.

- Microdispensing

This technique is well known from printing industry. Microdispensing of a sensor droplet is done with a piezo-electric tappet, which drives the cocktail from a reservoir through a nozzle. The method is suitable for viscous sensor cocktails and thickness can be controlled via repetition of the microdispensing or variation of the viscosity. With this method it is possible to directly print the spots into the MBR channels. [13]

Another method is the use of sensor beads or particles which can be applied to the medium after assemblage of the MBR. Particles might yield high signal strength, but they have to be dispersed into the medium and must not interact with the cells. There is the need of a sufficient amount of particles at one spot for a good read out signal. This might be achieved by the use of magnetic particles. [13]

2 Materials and Methods

2.1 Materials

Table 2: Chemicals used for the experiments.

Substance	Supplier	Purity	Comment
Polydimethylsiloxane (PDMS)	ABCR		MW 28000 Vinylsiloxy terminated 1000 cSt
Dimethylsiloxane-ethyleneoxide block copolymer (25 % non-siloxane) (DMS)	ABCR		400 cSt
Dimethylsiloxane-ethyleneoxide block copolymer (50-55 % non-siloxane)	ABCR		100 cSt
Hexamethyldisiloxane (HMS)	ABCR	98 %	
D4 hydrogel	HydroMed		
monoOH azaBODIPY	Self made [3]		
(25-35 % Methylhydroxysiloxane) dimethylsiloxane copolymer	ABCR		25 – 35 cSt
1,3,5,7-Tetravinyl-1,3,5,7-tetramethylcyclotetrasiloxane	ABCR	97 %	
Platinum(0)-1,3-divinyl-1,1,3,3-tetramethyldisiloxane complex	Aldrich		In xylene, ~2 % Pt
Egyptian blue (EB)	Self made [34]		EB B6 grob, tnb/sb Functionalized with 1H,1H,2H,2H-perflouroctyldimethyl-chlorosilane or TMS-Cl
Perflouroctyl-dimethylchlorosilane	ABCR	97 %	
Trimethylsilylchloride (TMS-Cl)	Sigma		
TiO_2 P170	Kemira		Ultrafine TiO_2
$CsCO_3$	Aldrich	99 %	
Tris	Roth	≥ 99.9 %	
NaCl	VWR Chemicals		

PS-Particles (O_2)	Self made [35]		Dye: platinum(II)-meso-tetra(4-fluorophenyl)tetra-benzoporphyrin (PtTPTBPF)
Cl-OH complex (pH)	Self made [4]		
K_2HPO_4	Roth	≥ 98 %	
KH_2PO_4	Roth	≥ 98 %	
Yeast Extract	Roth		for bacteriology
Peptone	Fluka		from soy been

2.2 Methods – sensor preparation

2.2.1 Preparation of Egyptian blue

Egyptian Blue particles (EB B6 grob tnb/sb) had already been prepared as described by Borisov *et al*. [34] The particles were functionalized with 1H,1H,2H,2H-perflourooctyl-dimethylchlorosilane. For that they (~356 mg) were weighted into a 15 mL Falcon tube, then the tube was filled with argon and tightly closed. Dry THF (approximately 1 mL) was added with a syringe under N_2 atmosphere and then perflourooctyldimethylchlorosilane (100 µL) was added. The suspension was sonified for 10 min and then stirred for another 20 min to obtain a homogenous suspension. The suspension was centrifuged (4000 rpm, 2 min) and the green supernatant was removed. Afterwards the particles were washed with acetone (2 times, 10 mL each) and EtOH (2 times, 10 mL each). After all washing steps a clear and colourless supernatant was obtained and discarded. The particles were dried at 70 °C over night and the dry particles were pestled.

2.2.2 Preparation of $CsHCO_3$

$CsCO_3$ (~1 g) was dissolved in ddH_2O (~5 mL) and the solution was gassed with CO_2 over night, until the majority of water was evaporated. Precipitation of white crystals was observed. To remove residual water the crystals were dried under N_2 and then a stock solution (100 mg/mL MeOH) was prepared.

2.2.3 Preparation of CO_2 sensors - knife coated foils

The development of the optical CO_2 sensors was based on an emulsion system using PDMS, and either D4 or DMS as emulsifier and monoOH azaBODIPY as CO_2 sensitive dye.

The monoOH azaBODIPY had already been prepared beforehand according to the synthesis methods described by Jokic *et al*. [3]

A standard composition of the sensors is summarized in Table 3.

Table 3: Composition of the two different emulsions used for sensor preparation.

Compound	Emulsion based on D4		Emulsion based on DMS	
	Amount [mg]	**Ratio***	**Amount [mg]**	**Ratio***
PDMS	500 mg		500 mg	
D4 (10 wt% in EtOH/H_2O 9:1)	500 mg	1:10 (D4:PDMS)	-	-
DMS (25 % non-siloxane)	-	-	50 mg	1:10 (DMS:PDMS)
monoOH azaBODIPY (2 mg/g THF)	100 mg	0.4 %(D4)	0.2 mg	0.4 %(DMS)
HMS	250 mg	1:2 (HMS:PDMS)	-	
CO_2	Solution gassed for around 30 s with 100 % CO_2			
$CsHCO_3$ (100 mg/mL MeOH)	50 µL	250 mM (D4)	25 µL	250 mM (DMS)
Egyptian Blue	5 mg	1:10 (EB:D4)	5 mg	1:10 (EB:DMS)
Copolymer	20 µL		20 µL	
Polymerisation retardant (10 % in cyclohexane)	10 µL		10 µL	
Catalyst	5 µL		5 µL	

*weight base

The emulsions were prepared as follows: The monoOH azaBODIPY stock solution was weighted and solvent was removed by evaporation under N_2. Afterwards the dye was dissolved in D4-stock or DMS (dissolved in 50 µL EtOH). Next the solution was gassed with CO_2 and $CsHCO_3$ stock was added. The solution was mixed thoroughly and afterwards PDMS was added. The emulsion was stirred with a KPG stirrer (IKA Werke) at 2000 rpm for around 15 min. The cocktail was heated to 105 °C to remove the solvent and thereafter the D4 emulsion was diluted with HMS. This was only done when sensors were prepared with D4. When DMS was used, addition of HMS led to an instable emulsion and hence was omitted. Last, Egyptian Blue was added and the emulsion was again stirred for around 15 min at RT for complete dispersion of EB into the emulsion.

The copolymer, polymerisation retardant and catalyst were added one after the other under rigorous stirring to initiate the polymerization of PDMS.

The emulsion was knife coated directly after addition of the catalyst. A Mylar® foil functionalized with siloxane was used for knife coating. The obtained foils were used for testing the sensors. When D4 was used, the foils were completely polymerized after around 20 min. On the other hand, polymerization with DMS took around 90 min. In this case the foil was warmed with a heat gun for around 2 min, approximately 45 min after initialization of the polymerization. Then it was incubated at 60 °C for at least 1 hour, to ensure a complete polymerization.

Usually the foils were knife coated with 1 MIL and after complete polymerisation a layer of TiO_2:PDMS:cyclohexane 1:1:2 was added. Polymerisation of PDMS was done in the same way as for the emulsions and again film thickness of 1 MIL was chosen for knife coating.

2.2.4 Dip coating of CO_2 sensor spots

The emulsion with DMS was used as described in chapter 2.2.3, Table 3, for dip coating of the CO_2 sensors. Polymerization was done according to the protocol used for knife coating. However, polycarbonate slides were used as substrate. Little recesses were drilled into the slides to ensure a good adhesion and to prevent spreading of the sensor spots. This was done with a borer connected to a CNC machine to ensure the right position and same size at all substrates. The depth was around 200 µm and the diameter 1.2 mm.

A CNC machine, composed of a CNC microstep driver (Benezan Electronics, Triple BEAST) and an axis motor (Isert electronics), as described in the master thesis of Sulzer, was used for exact and reproducible dip coating of the sensors. [36] The prepared emulsion (including polymerization reagents) was filled into a small scale pan, which was fixed under the arm of the CNC machine. A 10 µL pipette tip was fixed at the arm of the CNC machine in a way that it could just dip into the emulsion. Coordinates were set using the program LinuxCNC to ensure exact placing of the sensor spots on the substrate. The pipette tip was first dipped into the emulsion and then placed into the recess of the substrate. Dipping into the emulsion was done for 0.2 s; beside that no waiting times were set.

The time slot for dip coating was around 10 – 60 min after addition of polymerization reagents. Afterwards, the emulsion was not applicable anymore due to the high viscosity. Other than for the sensor foils no protective layer of TiO_2 was spotted onto the sensors. The risk of formation of inhomogenous sensor spots was too high.

2.2.5 Preparation of pH and O_2 sensors

2.2.5.1 Composition of the sensor cocktails

For the preparation of the pH sensor Cl-OH butoxy complex was used as described by Strobl *et al.* [4] The dye was dissolved in THF (2 mg/g THF stock solution) and as matrix D4 was used {8 wt% in EtOH/H_2O [9:1(v/v)]}. The dye stock solution was mixed with the D4 stock in order to obtain a final concentration of 0.3 % dye based on D4. Finally, Egyptian blue, functionalized with TMS-Cl, was added to the cocktail in a ratio of 1:2 [EB:D4(w/w)]. The cocktail was vortexed and sonified (Branson Digital Sonifier W-450D) to obtain a homogeneous suspension, according to the following protocol (Table 4).

Table 4: Protocol for sonication of the pH and O_2 cocktail.

total time	16 s
puls on	2.5 s
puls off	6.4 s
amplification	25 %

PtTPTBPF incorporated into PS particles was used for the O_2 sensors. The particles were prepared as described by Nacht *et al.* [35] The PS particles were mixed with D4 [5 wt% in Isopropanol:H_2O (3:1)] in a ratio of 1:1 [D4:PS (w/w)]. The suspension was vortexed and sonified in the same way as the pH cocktail (Table 4).

2.2.5.2 Preparation of the sensor spots

O_2 and pH sensor spots were prepared by spotting using the CNC machine, as described by Sulzer. [36] Again, a recess into the substrate was made with the CNC borer for an improved adhesion of the spots (as described in chapter 2.2.4). The diameter was 0.4 mm and the depth 0.2 mm, respectively.

The cocktail was filled into the syringe connected to the CNC machine and the CNC machine was connected with the microdispenser and its control unit (VERMES, MDV 3200A-HS-UF and MDC3200+). Spotting was done through a 70 µm nozzle and following parameters were used (Table 5).

Table 5: Parameters set for spotting the O_2 and pH sensor cocktails.

	O_2 sensor	**pH sensor**
pressure [bar]	1	1
tappet lift [%]	85	85
rising time [s]	0.6	0.3
opening time [s]	0.1	0.1
falling time [s]	0.09	0.05
delay [s]	0.1	0.1
number of pulses	3	5
number of spots	2	2 x 3

2.3 Methods – sensor characterization and analytics

2.3.1 Characterization of concentration rage and stability

Figure 6 shows the general set-up for the characterization of the sensor foils. This was used to estimate the concentration range, stability of the sensor, potential drifts or conditioning time.

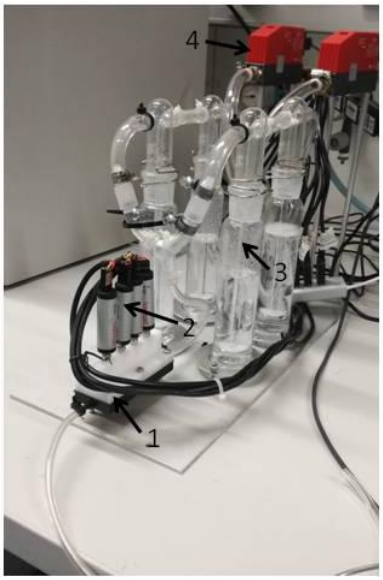

Figure 6: General set-up for characterization of the sensor foils. Tests were performed in liquid or gas phase, between 0 and 20 % CO_2 concentration. 1 measurement cell; 2 PICCOLOS; 3 gas washing bottles; 4 MFC

Incoming gas flow (air and CO_2) was controlled with a mass flow controller (MFC) (Vögtlin, red-y for gasflow GSC-A4TA-BB22) to adjust the proper CO_2 concentration. The MFC controlling the gas flow rate was operated with the program LabView (Pyro Science). After the gas flow was adjusted, the gases were humidified with water by two gas-washing bottles, each. Thereafter the gases were mixed and bubbled through the measurement cell. Four PICCOLOS (Pyro Science, optical oxygen meter) were used for measurements of phase angles and intensities over time.

Measurements were usually done between 0.04 % (air) and 20 % CO_2, measuring five concentration steps (30 min per step). The foil was fixed into the measuring cell in front of the PICCOLOS and tests were performed in Tris-buffer [20 mM, pH 7.4 (at RT), 150 mM NaCl] or in gas phase at RT, 30 °C or 37 °C, respectively. Measurements at 30 °C or 37 °C were done in the same the set-up, placed into a heating cabinet (Memmert).

2.3.2 Response time measurements

Figure 7 shows the set-up used for determination of the response time in liquid phase.

Figure 7: General set-up for measuring response times. In a Schott flask the buffer was saturated with CO_2 (5 or 15 %). The buffer was then manually pumped into a flow-through cell containing the sensor foil. 1 syringe; 2 Schott flask with buffer; 3 MFC; 4 flow through cell; 5 PICCOLO.

Measurements for determination of the response time were done at RT, 30 °C and 37 °C in Tris-buffer [20 mM, pH 7.4 (at RT), 150 mM NaCl]. Response time was investigated between 5 and 15 % CO_2. The set-up is composed of a Schott flask (100 mL) filled with buffer. Two MFC (for CO_2 and N_2) are connected to the flask by a gas tight tube to set the gas concentration. The flask is further connected to a flow through cell (containing the sensor foil and ~2 mL liquid volume). Measurements of the phase angle were done with a PICCOLO, which was fixed at a defined position on the sensor foil. The program Oxygen Logger (Pyro Science) was used for read out of the PICCOLO signal.

The Scott flask was filled with buffer and saturated with CO_2 (5 or 15 %) for at least 30 min under rigorous stirring. Afterwards a syringe was used to manually pump (two times, 10 mL each) buffer with defined CO_2 concentration into the flow through cell. The quick exchange of the buffer results in an immediate change of the CO_2 concentration, avoiding delays due to equilibration, and hence response time could be determined. The phase angle was measured and t(90) was calculated.

2.4 Methods – sensor application in microbioreactor

2.4.1 Design of the sensor slide

Figure 8 shows the sensor plate used for application in the MBR. As described in chapter 2.2.4 the CO_2 sensors were dip coated while O_2 and pH sensors were spotted onto the substrate. The substrate is made of polycarbonate and for each sensor spot a small recess was made for improved adhesion. A diameter of ~1.2 mm was chosen for the CO_2 sensors, while the diameter is 0.4 mm for O_2 and pH with a depth of 0.2 mm, each. The slide is 7.5x2.5 cm long, the distance between lower end and pH spot is 15 mm. The distance between the pH, O_2 and CO_2(l) spots is 5 mm, each. Between the CO_2(l) and CO_2(g) spots there is a distance of 20 mm. The position of the pH, O_2 and CO_2(l) spot is arranged in a way that they are covered with liquid if a minimum reaction volume of 500 µL is used. The CO_2(g) spot is placed in a manner that its position is at the upper end of the reactor just before the gas exit of the MBR. The section above the CO_2(g) spot is not part of the reactor anymore and was usually cut so that the plate fits perfectly into the MBR.

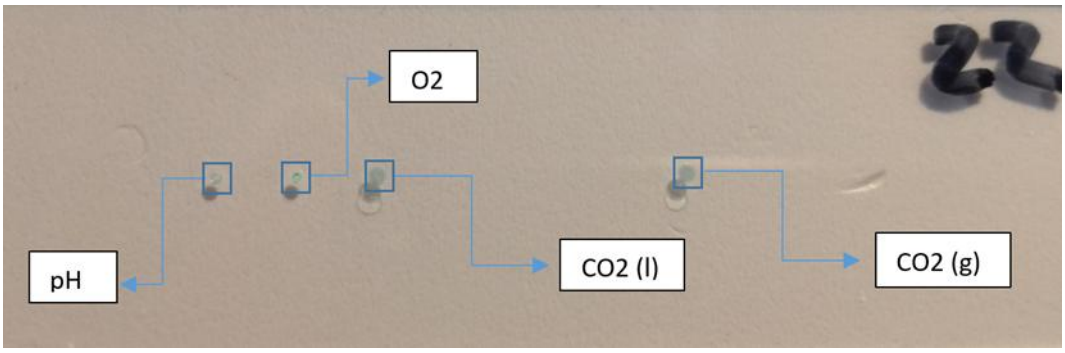

Figure 8: Sensorspots on polycarbonate substrate. pH, O_2 and CO_2 for measuring in liquid and gas phase.

2.4.2 Design of the reactor

Figure 9 shows the different parts of the MBR used for sensor spot characterization and cultivation of *S. carnosus* and *S. cerevisiae*.

Figure 9: Microbioreactor design: Different parts of the microreactor used for cultivation. 1 microreactor inner view, 1a connection for cooling water, 1b gas in/outlet; 2 microreactor front site; 3 sealing; 4 connector for filling; 5 backside of the reactor composed of a holder and the sensorplate; 6 reactor – back view – including sealing and sensorplate; 7 whole reactor with sensorplate and connector fixed into the docking station providing connection to the cooling system and glass fibres; 8 docking station – front view – stationary part for fixation of the reactor system; 9 docking station – back view – the docking station provides connections to the cooling system and enables positioning of the glass fibres and temperature sensor.

The MBR itself is a 3D-printed device (designed and printed at Leibniz Universität Hannover, Institut für Technische Chemie, Jan-Luca Lohse), made up of polyacrylate and consists of four main parts (Figure 9). There is the docking station (Figure 9 – nr 8 and 9), which is permanently connected to the measurement station [MFC, water bath, glass fibres and Firesting (Pyro Science)]. On this docking station the reactor itself can be fixed with screws. The two main parts are the MBR and the back including the sensor plate (Figure 9 – nr 1 and 5). In between there is a silicone-sealing (Figure 9 – nr 6) and these parts are connected with magnets. The MBR is equipped with a double jacket and connected to the water bath for regulation of the reaction temperature (Figure 9 – nr 1a). Further, there are in- and outlets for gas (Figure 9 - nr 1b) and a reaction chamber (Figure 9 - nr 1c). The reaction chamber can be charged and emptied by using the connector (Figure 9 - nr 3).

2.4.3 Measurement set-up

Figure 10 shows the measuring set-up of calibration and cultivation in the reactor.

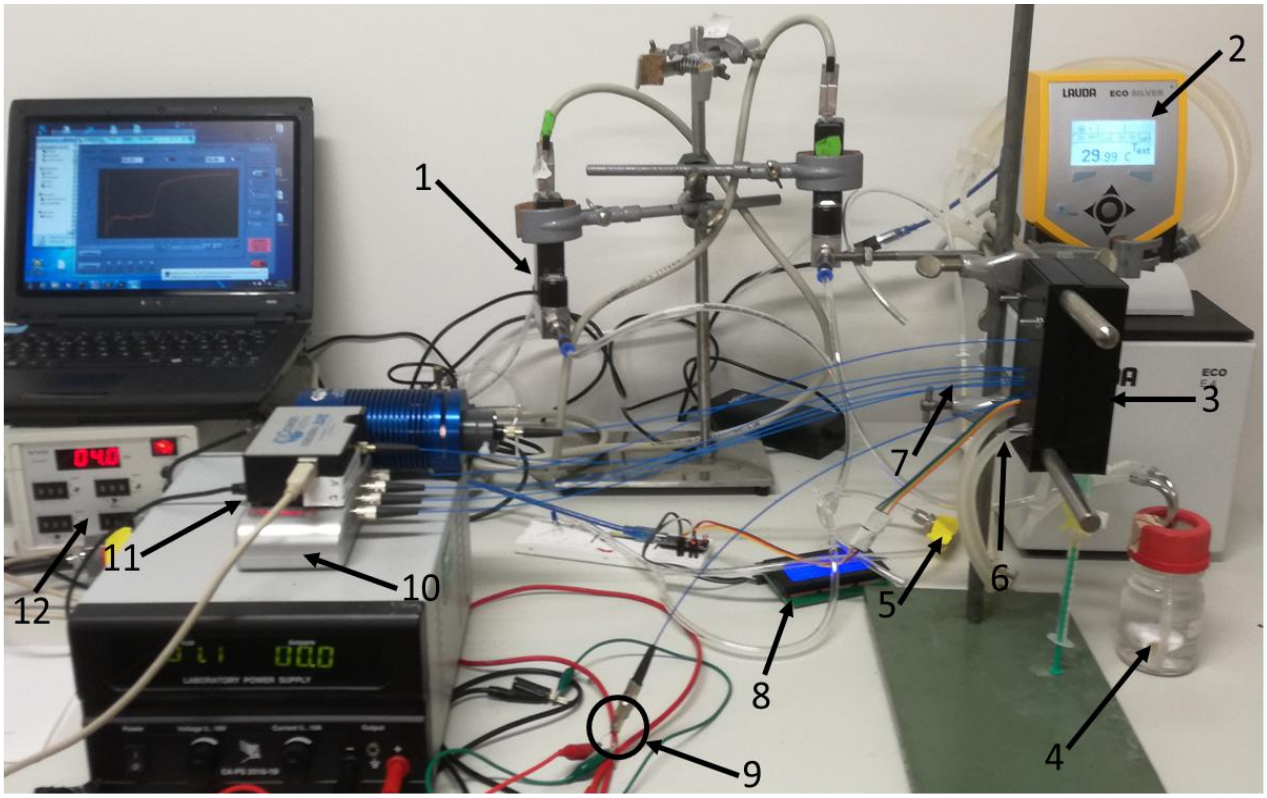

Figure 10: Measurement set-up for cultivation and calibration in the MBR. 1 Mass flow controller; 2 thermostat; 3 reactor with opaque cover; 4 Scott flask with water to humidify incoming gas; 5 pressure valve for regulation of the gas flow; 6 connections of cooling water to reactor; 7 glass fibres; 8 temperature control for the reactor; 9 LED for scattered light measurement; 10 Firesting; 11 Ocean optics; 12 controller to set mass flow.

Two MFC (Brooks; Model 5850TR) (Figure 10, nr 1) were used for calibration with air and CO_2, respectively. A WMR compact 4 controller (Figure 10, nr 12) was used to regulate the gas flow. Additionally a pressure valve (Figure 10, nr 5) was used to reduce the gas flow (of the mixed gas) from around 150 mL/min (mixture of air and CO_2) to 10 mL/min (entry to the reactor). The minimal mass flow of the MFCs is at around 2.5 mL/min and therefore a high total mass flow of 150 mL/min was used to ensure an accurate calibration. Reduction of the flow to 10 mL/min was necessary in order to prevent evaporation and sputtering of the liquid. A third MFC (Red-y for gas flow, Vögtlin instruments; not shown) was needed to regulate the excess of air/CO_2 resulting from reduction of the mass flow through the pressure valve.

All connections for gas inlet were achieved with gas tight tubes, made of polyether-polyurethane. Calibrations were done with dry gas, while the air was humidified for cultivation, using a Schott flask filled with ddH_2O (Figure 10, nr 6), in order to reduce evaporation of the reaction media. Aeration during the cultivation was done with only one MFC, which was set to 10 mL/min.

The temperature was regulated through a thermostat (LAUDA, Eco Silver) (Figure 10, nr 2), connected to the double jacket of the reactor (Figure 10, nr 12). Further, temperature of the reactor was externally measured (Figure 10, nr 8) using an infrared temperature sensor (MLX90614, Melexis NV).

During cultivation and calibration phase angles of the CO_2, O_2 and pH sensors were measured with a FIRESTING (Pyro Science). Excitation was done at 640 nm using glass fibres with a diameter of 800 µm and a length of 0.5 m (Figure 10, nr 7, nr 10). All signals were recorded with oxygen logger (Pyro Science). Following parameters were used (Table 6):

Table 6: Parameter set for measuring fluorescent signal of CO_2, O_2 and pH sensor.

Sensor	Frequency [Hz]	Amplification	LED intensity [%]
CO_2	2000	400x	100
pH	2000	400x	100
O_2	4000	400x	40

OD_{600} was estimated by scattered light measurements using an Ocean optics USB 2000 XR combined with a red LED (Figure 10, nr. 11 and 9). For that an LED with an emission maximum of 640 nm was used and the intensity was set to 1.7 VOLT. A glass fibre connected to the LED was placed in the reactor and the scattered light resulting from excitation with the

LED was measured with the Ocean optics. Measurements were done in the dark and the MBR was covered with an opaque, black cover (Figure 10, nr 3), to prevent interferences with light.

2.4.4 Calibration of sensor spots and scattered light

Concentrations in the range from 1.5 – 25 % were used for the calibration of CO_2 sensors. Lower CO_2 concentrations were not calibrated since with 1.5 % the lower limit of the MFC was reached. The MFCs are calibrated for air. The mass flow of CO_2 was calculated based on the conversion factor (CF) given by the user manual of Brooks instruments (equ. 26 and 27).

$$MF_{CO2(100\%)} = MF_{air(100\%)} * CF \quad \text{equ.26}$$

$$MF_{CO2(100\%)} = 250\ mL/min * 0.773 = 193.25\ mL/min \quad \text{equ.27}$$

Mass flow was defined in percent, where 250 mL/min air equals 100 %. According to the CF, 100 % CO_2 equals a flow of 193.25 mL/min. Based on these values, mass flow and percentage values were calculated for CO_2 and air at 150 mL/min mass flow (Table 7).

Table 7: Concentration range used for calibration and calculations to set correct values for mass flow controllers.

cCO_2 [%]	**Mass flow CO_2 [ml/min]**	**% mass flow CO_2**	**Mass flow air [ml/min]**	**% mass flow air**
1.5	2.25	1.2	147.75	59.1
2	3	1.6	147	58.8
3	4.5	23	145.5	58.2
5	7.5	3.9	142. 5	57
7.5	11.25	5.8	138.75	55.5
10	15	7.8	135	54
15	22.5	11.6	127.5	51
20	30	15.5	120	48
25	37.5	19.4	112.5	45

Dry gas was used to reduce equilibration times for calibration of the CO_2 concentration. The used concentration steps are shown in Table 7. Calibrations were done at the cultivation temperature (usually 37 °C) and in KPi-buffer (pH 7.4, 0.1 M). The sensors were first conditioned at 5 % CO_2 for at least 3 h, usually over night. The gas mixture with the right concentration was bubbled through the reactor at 10 mL/min. Calibration was started with increasing CO_2 concentrations and then the concentration was decreased again. Each concentration step was held until a stable signal was obtained. To ensure stable and reproducible values, at least one complete cycle (increasing and decreasing CO_2

concentration) was measured. If the measurements were instable, a second cycle was performed.

A two point calibration of the O_2 sensor was done at 0 and 100 % air. For that the reactor was bubbled either with 100 % air or 100 % CO_2.

Calibration of the pH spots was done with six different solutions of KPi buffer (0.1 M) in the range of pH 4.5 – 8.4. Calibration was also done at reaction temperature. Table 8 shows the pH values used for calibration, according to the reaction temperature.

Table 8: pH values used for calibration at the two reaction temperatures.

pH (RT)	pH (30 °C)	pH (37 °C)
4.5	4.52	4.61
5.4	5.5	5.51
6.02	6.21	6.17
6.82	6.98	7.03
7.4	7.61	7.55
8.64	8.7	8.72

The buffer solutions were heated prior to calibration. Calibration was done with increasing pH and at each pH point calibration was done until a stable signal was obtained. Then the buffer solutions were exchanged with a syringe.

Correlation of OD_{600} to scattered light was done for cultivation with *S. carnosus*. Cultivation with 2 mL reaction volume was started in order to ensure enough volume for sampling. The cultivation conditions were kept constant (37 °C, 10 mL/min aeration, start at OD_{600} of 0.1). OD_{600} was measured at the start and end point. Additionally, every 2 h a sample was taken with a syringe (~50 µL), diluted and OD_{600} was measured with a spectrophotometer (Biochrom, libra s11). The measured OD_{600} values were then correlated to the scattered light signal.

2.4.5 Cultivation in the microbioreactor

S. carnosus and *S. cerevisiae* were used for cultivation in the MBR, respectively. In both cases first a pre-culture was cultivated in a chicane flask and then cultivation of the main culture was done in the MBR at appropriate reaction conditions. Around 1 mL cultivation volume was used in order to prevent strong evaporation. The culture was gassed with humidified air (10 mL/min) to ensure O_2 supply.

2.4.5.1 Cultivation of S. carnosus

S. carnosus TM300 GFP was used for cultivation in the MBR. The organism contains the following plasmid: pCX-pp-sfGFP, which would enable GFP production by induction with xylose. In this study no protein expression was induced and only growth of the organism related to O_2 and CO_2 concentration as well as pH was investigated. Cultivation was done in LB media (Table 9) as described by Krull. [37]

Table 9: Composition of LB media for cultivation of *S. carnosus*.

Component	Concentration [g/L]	Sterilization
Yeast extract	10	Autoclave together, 120 °C, 20 min
Peptone	20	
NaCl	10	
K_2HPO_4	0.684	
KH_2PO_4	0.247	
Glucose	1	Autoclave separately, 120 °C, 20 min
Chloramphenicol	0.01 (1 g/L stock solution)	Sterile filtration 2 µm

The pre-culture was done in a chicane flask (100 mL) filled with LB media (10 mL) and Chloramphenicol (100 µL stock solution) and it was inoculated with a pipette tip of a cryogenic culture of *S. carnosus*. Cultivation was done at 37 °C and 180 rpm for 10 – 12 h, resulting in an OD_{600} of around 20.

Afterwards a main culture was inoculated to an OD_{600} of 0.1 using the same media as for the pre-culture. The culture broth (1 mL) was filled into the MBR and measurements were directly started. Temperature was set to 37 °C and aeration to 10 mL/min. In addition, the rest of the culture was cultivated in the shaking flask as reaction control. Cultivation was done until a stationary phase was reached (usually 12 -14 h).

2.4.5.2 Cultivation of S. cerevisiae

S. cerevisiae N 34 was used as second culture to investigate performance of the sensors in fermentations. Cultivation was done as described by Hönnscheidt. [38] Table 10 shows the composition of the media used for cultivation. The pH of the media was adjusted to 5.5.

Table 10: Composition of the LB-complex medium used for cultivation of *S. cerevisiae*.

Component	Concentration [g/L]	Sterilization
KH2PO4	14.2	Autoclave together, 120 °C, 20 min
Na2HPO4	0.8	
Yeast extract	5	
Peptone bacteriological	5	
Glucose	7.5	Autoclave separately, 120 °C, 20 min

The media (10 mL) was filled into a chicane flask (100 mL) and inoculated with cryogenic culture (1 mL) for the pre-culture. Cultivation was done at 30 °C and 150 rpm for 15 h, resulting in an OD_{600} of ~4.

Inoculation of the main culture was done to an OD_{600} of 0.1 and the culture broth (1 mL) was filled into the MBR. Measurements were directly started and the culture was aerated with 10 mL/min. Temperature was regulated to 30 °C and cultivation was done for more than 24 h to ensure stationary phase of the cell growth. Again a culture in the shaking flask was done as control.

2.4.6 Stability measurements

Equilibration, calibration and cultivation were done in the MBR using the set-up as described in chapter 2.4.3. Further, measurements on long term stability of the CO_2 sensors were done. For that, experiments were performed in a CO_2 incubator (Heracell 150i, Thermo) at constant conditions of 5 % CO_2, 100 % humidity and 37 °C. Measurements were done in liquid and gas phase for at least one week. For read out of the sensor a PICCOLO (Pyro Science) connected to oxygen logger (Pyro Science) was applied, using the parameter as described in chapter 2.4.3, Table 6. A holder for the PICCOLO was designed for the measurements in gas phase and conditions in the incubator were kept constant. Measurements in the liquid phase were done using the set-up as shown in Figure 11.

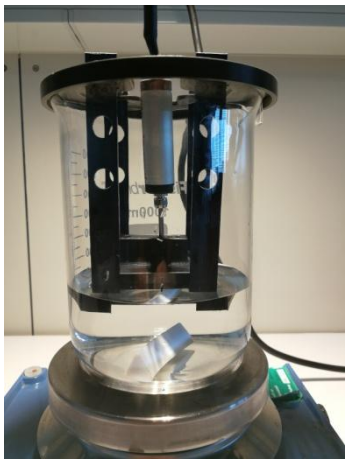

Figure 11: Set-up for stability measurements of the sensor in liquid phase in the incubator (100 % humidity, 5 % CO_2, 37 °C).

A beaker was filled with water and stirred at 100 rpm for at least 2 h to equilibrate. Then the sensor plate was put into the solution and measurements were again performed at constant conditions.

3 Results and discussion

3.1 Sensor development and preliminary characterization

The aim of this study was to develop a CO_2 sensor for application in the MBR. The developed sensors were based on an emulsion system using PDMS as matrix and monoOH azaBODIPY as CO_2 sensitive dye. First, it was investigated how different $CsHCO_3$ concentrations and different reagents (D4 or DMS) for incorporation of the dye into the matrix influence the sensor performance.

3.1.1 Investigation of the CO_2 sensor composition

The sensor performance was investigated with the set-up as described in chapter 2.3.1. The phase angles were measured over time for the different sensor foils.

First the sensors based on D4 were characterized. The influence of the $CsHCO_3$ concentration (150 or 250 mM), the film thickness (0.5 or 1 MIL), dilution and addition of TiO_2 on the measurement was tested. These tests were done in liquid phase. Testing of sensor foils with D4 in gas phase were only done as proof of principle without dilution and without defined $CsHCO_3$ concentration and TiO_2 layer at 1 MIL film thickness (see appendix; Figure 28). No clear difference in phase shift, signal stability and signal drift was found by varying these parameters (see appendix; Figure 27, Figure 29). Hence, the film was layered with TiO_2 in order to enhance signal intensity. In order to facilitate the handling, sensors were diluted 2:1 (PDMS:HMS), which also seems to improve sensor performance (see appendix; Figure 29). The sensor films were knife coated with 1 MIL, resulting in a thickness of around 10 – 12 µm. $CsHCO_3$ in a concentration of 250 mM was added in order to ensure a sufficient amount of base and hence a broader dynamic range. [20]

Sensor foils composed of D4 needed an equilibrium phase of 5 h to 10 h to achieve reasonably stable signals by variation of the CO_2 concentration. However, the signal still drifted over time and over a measurement period of around 20 h and did not become completely stable. Drifts were observed at RT, 30 °C and 37 °C in liquid and gas phase. Figure 12 shows a typical example for the characteristic response of the sensor in liquid phase at 25 °C.

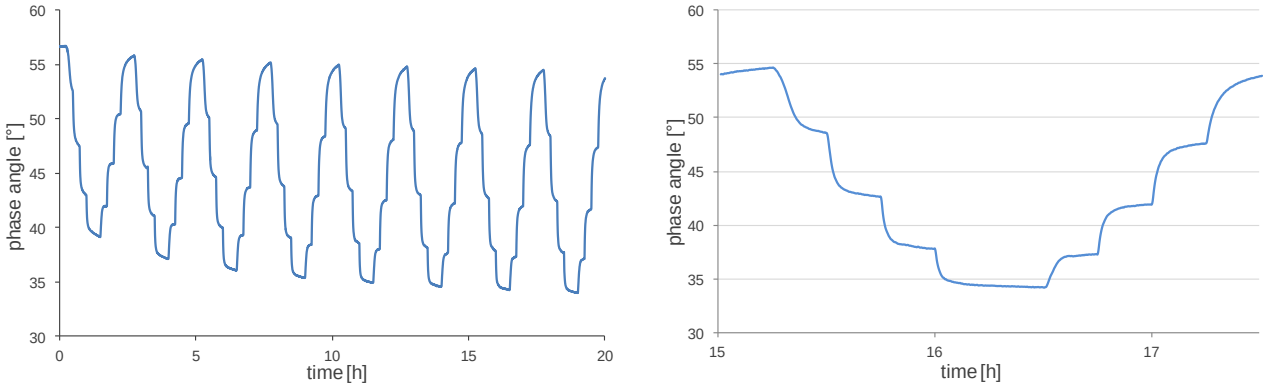

Figure 12: Sensorfoil, PDMS:D4 (10:1), 250 mM $CsHCO_3$, 0.4 % monoOH, 10 % EB, dilution 2:1 (PDMS:HMS), 1 MIL, TiO_2, measured in Tris-buffer at 25 °C. Left: complete measurement; right: 7th cycle.

Throughout the first cycle the single steps were difficult to distinguish and it rather looks like a continuous decrease in phase angle. After 1 – 2 hours the steps became discrete and more stable, however, within the first three – four cycles (~10 h) there was a strong drift towards lower phase angles. The difference in phase angle at 20 % CO_2 between the first and the 4th cycle was 4.5°, while from the 4th to the last cycle the difference was reduced to 1.4°. Further, the last cycle showed quite stable signals. The single steps were easy to distinguish and the difference between the signals at the same concentration when lowering or raising the concentration was between 0.3° and 1.2°, depending on the concentration (Figure 12, right).

D4 is a material that takes up around 50 % water [39], which is necessary for the function of the sensor [15][26][40], hence it was assumed that equilibration is caused by humidification of the sensor. Therefore, the possibility to overcome this phenomenon was tested by incorporating the dye directly into PDMS with support of an emulsifier. DMS was used as emulsifier, which is insoluble in water [41] and it is assumed that only small amounts of water are taken up by this substance. [42] Sensor foils were prepared using DMS with 55 % or 25 % non-siloxane groups. Dilution of an emulsion based on DMS with HMS resulted in an inhomogeneous emulsion. Inhomogeneity was worse when 55 % non-siloxane DMS was used. Hence, emulsions were prepared with 25 % non-siloxane DMS and without any dilution. Furthermore, polymerization time was much longer when using DMS instead of D4. Polymerization took around 2 h (instead of 15 min) and it was necessary to treat the foil with heat (1 min heatgun and 2 h at 60 °C). It seems that the ethyleneoxide part of DMS prevents polymerization due to surfactant properties.

As with the previous system using D4, tests were performed at RT, 30 °C and 37 °C. This system also showed a signal drift and a conditioning phase was necessary. However, in this

case conditioning was much shorter, resulting in a stable signal after around 3 – 5 h. Further, it seems that the drift in general is lower and stabilization of the signal is faster.

Figure 13 shows one example of a sensor foil using DMS characterized at RT in liquid phase.

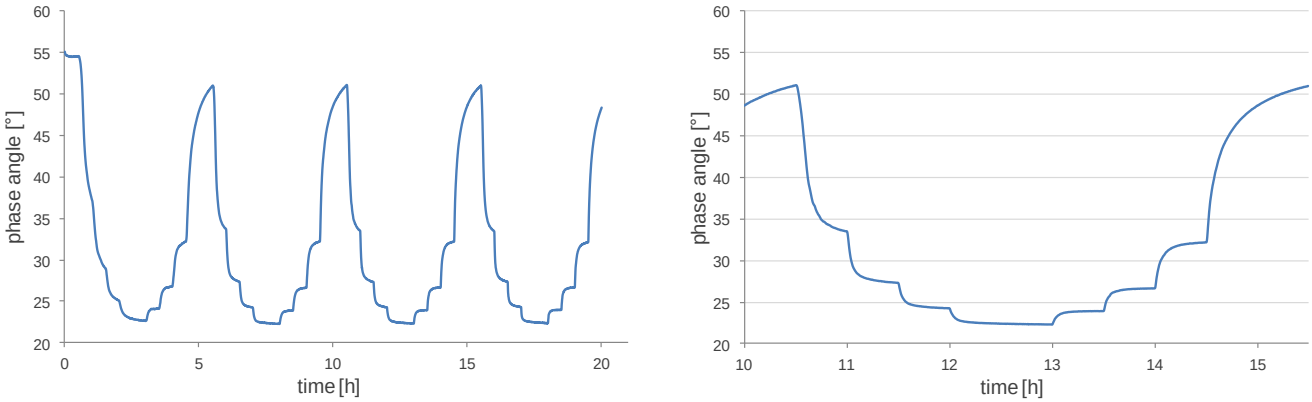

Figure 13: Sensorfoil, PDMS:DMS (10:1), 250 mM $CsHCO_3$, 0.4 % monoOH, 10 % EB, 1 MIL, TiO_2, measured in Tris-buffer at RT. Left: complete measurement; right: third cycle.

Again a short equilibration phase was needed in order to clearly distinguish between the concentrations and get stable signals. However, in this case the signals were almost stable with very little drift after 3 h (compared to D4, Figure 12). The difference in phase angles at 20 % CO_2 between first and last cycle was 0.3°, which is 5 times less compared to the foils with D4 (Figure 12). The differences in phase angles at the last cycle, comparing the same concentrations (Figure 13, right), was between 0.12 to 1°, which is similar to those of sensors with D4. In conclusion DMS facilitates equilibration compared to using D4 as host polymer. As already mentioned, water is essential for a functional CO_2 sensor [15][26][40] and therefore the need of a short equilibration time is reasonable in order to adjust the sensor from the dry condition during storage to humid measurement conditions. Since D4 takes up more water it is expected that equilibration takes longer than with DMS. Since conditioning time is shorter and signals are more stable further investigations were performed with the sensor system based on DMS.

3.1.2 Measurements in gas and liquid phase

Measurements in the gas phase as well as in the liquid phase are of interest for an application of CO_2 sensors in bioreactors. Previous studies showed that optical CO_2 sensors are able to measure CO_2 in gas phase [15][18][25][26][40] as well as dissolved CO_2 in liquid phase. [17][19] Application of the sensor set-up was tested in both phases. The concentration range of CO_2 in fermentations is expected to be between 5 – 15 % (liquid and gas

phase). [23b] As already shown in Figure 13 measurements in liquid phase are possible and the sensor response to concentrations between 0 and 20 % was stable after around 5 h. Testing of the sensor in gas phase was done analogously to liquid phase measurements by simply omitting the buffer (chapter 2.3.1).

Figure 14 shows the results obtained by characterization of the sensor foil in gas phase at RT.

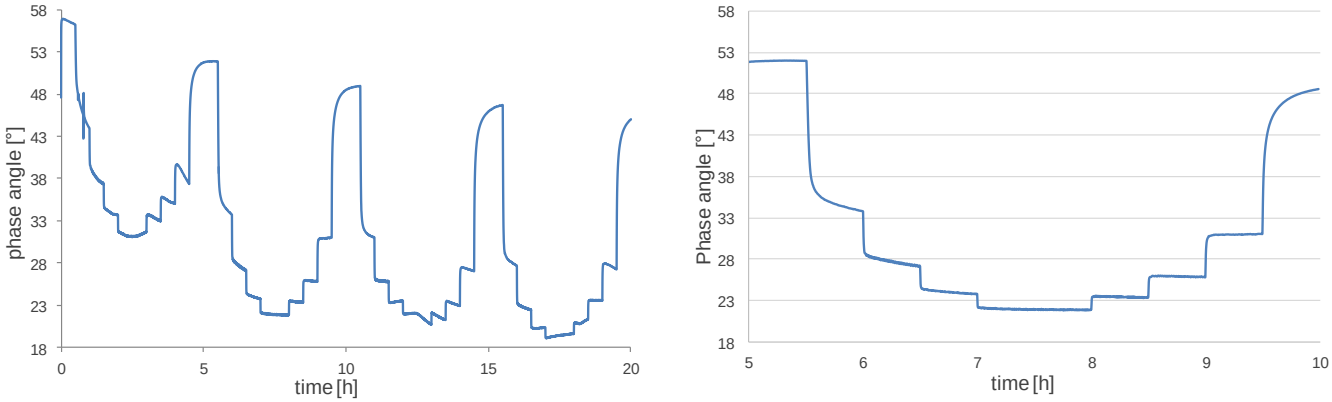

Figure 14: Sensorfoil, PDMS:DMS (10:1), 250 mM $CsHCO_3$, 0.4 % monoOH, 10 % EB, 1 MIL, TiO_2, measured in gas phase at RT. Left: complete measurement; right: third cycle.

Comparing this to the results obtained in liquid phase it is obvious that the signal is less stable. The sensor still showed a drift after 20 h and the signal was irregular. After 5 h the signal was getting stable, however, then it became instable again. At higher temperatures the drift became stronger and signals did not stabilize after 10 h, indicating that the gas phase measurements need a longer conditioning time than liquid phase. This might be due to longer time for humidification of the sensor compared to liquid phase measurements.

Although the sensors had not been stabilized after 10 h it has been shown that they respond to changing CO_2 concentrations and are hence usable for estimation of CO_2 concentrations in gas phase.

Due to the strong drift in gas phase it is difficult to compare the results with the liquid phase measurements. Anyhow, the response is similar as in liquid phase with phase angles in the range from around 50° to 20° (comparison to Figure 13).

Further, all sensors (D4 and DMS) in both, gas and liquid phase, showed a higher sensitivity for low CO_2 concentrations (Figure 12, Figure 13, Figure 14). Especially between 0 and 5 %, there are high differences in the phase shift. This was already expected, since it was shown

that CO_2 sensors mainly show a hyperbolic response and sensitivity decrease with increasing concentrations. [15][17][18][20][25][26][43][44]

3.1.3 Influences of temperature on measurements

Literature data show a temperature dependence of the CO_2 sensor response, which is mainly explained by decrease of CO_2 solubility at higher temperatures. [15][17][19][25][44] Hence also the influence of reaction temperature was tested. Measurements were done at RT, 30 °C and 37 °C (Chapter 2.3.1). Figure 15 shows the signals obtained with different CO_2 concentrations depending on the temperature in liquid phase. Measurements in the gas phase were not considered, due to high instabilities of the signal.

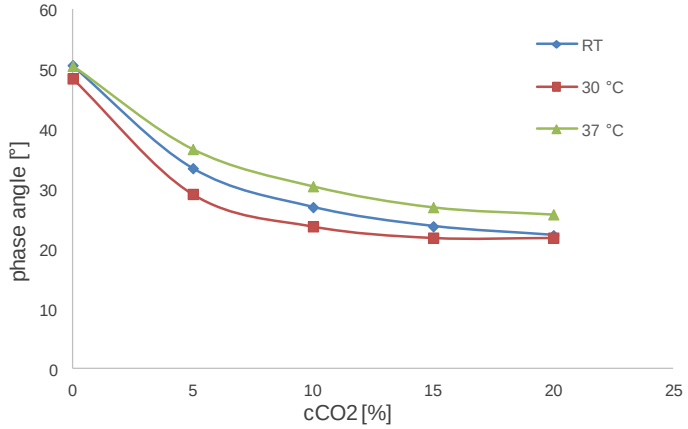

Figure 15: Phase angles at different CO_2 concentrations (0 – 20 %) and temperatures measured in Tris-HCl (0.1 M, pH 7.4).

Comparing the phase angles and differences between the CO_2 concentrations at different temperatures there was no significant trend observable. The sensors respond in the measuring range from 0 – 20 % CO_2 and phase angles were in the range from 50° – 20°, where phase angles were slightly higher at 37 °C. Further, as already shown, sensitivity increased with decreasing CO_2 concentrations. In conclusion the sensors can be used in the range of 20 to 37 °C without obvious differences. However, phase angles are different at the measured temperatures and the dye and reference particles are temperature dependent. [34] Hence, calibrations have to be done for each temperature.

3.1.4 Response time measurements

The response time was determined for liquid and gas phase at RT and 37 °C to further characterize the sensor properties (set-up chapter 2.3.2).

Results and discussion

Figure 16 shows the response times for the sensor foil in liquid and gas phase as well as for a sensorspot in liquid phase, at RT and 37 °C when decreasing or increasing the CO_2 concentration. In the appendix (Figure 30) a typical curve for the response time measurements is shown.

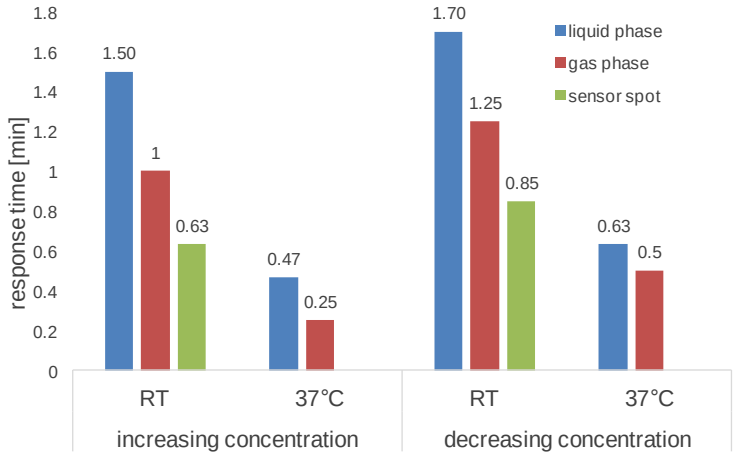

Figure 16: Comparison of response time of the sensorfoil in liquid and gas phase at RT and 37 °C as well as response time of a sensorspot in liquid phase at RT. PDMS:DMS (10:1), 250 mM $CsHCO_3$, 0.4 % monoOH, 10 % EB, 1 MIL, TiO_2, measured in Tris-buffer at RT. Changing CO_2 concentration from 5 to 15 %.

The response was faster in gas than in liquid phase and also when increasing the temperature from RT to 37 °C. Further, when the CO_2 concentration was increased the sensor responds faster than when the concentration was decreased. Both the temperature dependence [17] and dependence of the response time on used CO_2 concentrations was already expected. [15][17][25][26][40][43] Moreover, the sensor spot showed better response times than the foils for both liquid and gas phase experiments, which is probably due to better accessibility. The process is diffusion controlled [20] and hence it is probable that this is faster when providing a larger surface due to the spot compared to the foil. Fastest response time was at around 20 s, while slowest response was determined to be around 1.7 min. Response times for optical CO_2 sensors were reported between 3 and 100 s [15][25][40][43] and therefore the measured response times are reasonable. In comparison, commercial optical CO_2 sensors from PreSens state a $t_{90} < 3$ min at 20 °C for a change from 2 to 5 % CO_2. [45] Moreover, complete cultivation of *S. carnosus* needs more than 10 h. [37] Hence it can be assumed that an application in the MBR is feasible, especially since faster response is expected for the sensor spots.

3.2 Characterization of CO_2 sensor spots

After preliminary characterization of the sensor performance using sensor foils, the sensor spots were characterized in detail (preparation chapter 2.2.4). Stability, sensitivity, reproducibility and dependence on reaction media were estimated.

3.2.1 Sensor stability

As already observed with the sensor foils, there is a drift in the signal. Hence, it was investigated how the sensor signal evolves over time. For that stability tests were performed to estimate equilibration time and signal stability. Further, shelf life and operational stability were roughly estimated.

3.2.1.1 Equilibration time and stability

The time for complete equilibration of the sensor and the possibility to obtain a stable signal was investigated. For that the sensors were incubated at 5 % CO_2 concentration, 37 °C and 100 % humidity in gas phase or in liquid phase (set up Figure 11).

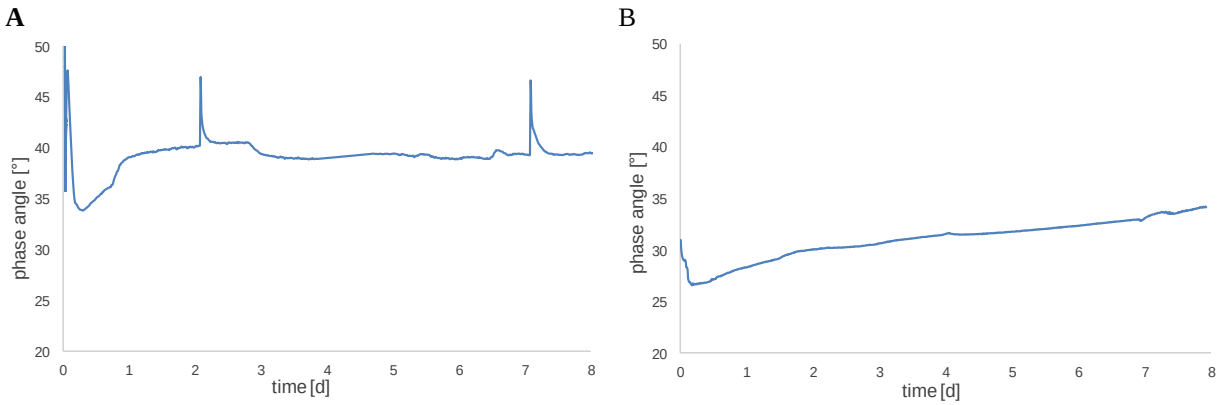

Figure 17: Investigation of long term stability of the CO_2 sensor in the gas phase (A) and water (B). Incubation of the sensors at 100 % humidity, 37 °C and 5 % CO_2. Continuous measurement over 8 days.

Figure 17A shows the stability measurements of the CO_2 sensor in the gas phase. The sensor first needs a conditioning time of about 10 h, where the sensor signal decreases continuously. This was already observed for the sensor foils (Figure 12, Figure 13, Figure 14). Over the next 10 – 12 h the sensor signal increased again and after one day it started to stabilize. The sensor signal was constant after 3 days and stable signals with little variation can be assumed after an equilibration phase of around 24 h. The peaks that can be observed at day 2 and day 7 are due to opening of the incubator followed by a decreasing CO_2 concentration. This indicates a fast

response of the CO_2 sensors and shows that the signal stabilizes again when the CO_2 has reached a constant value of 5 %.

Beside the equilibration phase, drifts of the sensor might be due to poisoning of the sensor. The base of the sensor can also react irreversibly with acidic gases [17], which can diffuse through the PDMS matrix. [17][46] Consequently this would result in decreasing phase angles. Also leaching or photobleaching of the sensor dye could cause a drift due to loss of luminophore intensity. This would change the ratio of the dye and EB and probably results in an increase in phase angle. [8][9][47]

Figure 17B shows the stability test in liquid phase. Other than in gas phase the signal drifted continuously towards higher phase angles. There was no stabilization over the measurement period and it seems that influences on the stability in liquid phase are higher than in gas phase. As observed in the gas phase the signal first decreased within the first hours, which is probably explained by an equilibration phase. The slope of increasing phase angle was constant over the first 2 days and then decreased and remained constant for day 2 to day 8.

The media in the gas phase does not change over time and all measured differences can be related to the CO_2 sensor. However, in liquid phase it cannot be excluded that changes of the media composition influence the sensor response. Corrosion of the used screws due to the experimental set-up was observed. Attempts were made to avoid rusting by using water instead of buffer and covering the screws with liquid rubber. This reduced the corrosion but it could not be completely avoided. Corrosion of iron can occur due to dissolved CO_2. The CO_2 reacts with water to form carbonic acid according to the CO_2 equilibrium in water (see equ. 10 – 13, chapter1.6.2) which can generate $FeCO_3$ (equ. 28 – 31).

$$Fe \rightarrow Fe^{2+} + 2e^{-} \qquad \text{equ.28}$$

$$Fe^{2+} + CO_3{}^{2-} \rightarrow FeCO_3 \qquad \text{equ.29}$$

$$Fe^{2+} + 2HCO_3{}^{-} \rightarrow Fe(HCO_3)_2 \qquad \text{equ.30}$$

$$Fe(HCO_3)_2 \rightarrow FeCO_3 + CO_2 + H_2O \qquad \text{equ.31}$$

Due to the presence of oxygen this can further oxidize to iron oxide or hydroxide. [48]–[51] The corrosion reactions might change the equilibrium of dissolved CO_2 resulting in decreased CO_2 concentration and hence in a continuous sensor drift. After finishing the stability test, the pH of the solution was measured. It increased from initially 4.9 (water incubated at 37 °C and 5 % CO_2) to 5.8. This indicates a decrease in CO_2 concentration due to $FeCO_3$ formation.

Further, similar as for the gas phase measurements poisoning, leaking or bleaching of the dye might result in the signal drift. [8][9][17][47] These effects might be accelerated due to the media composition.

Compared to that, Figure 18 shows the data from equilibration of all sensor spots at 37 °C and 5 % CO_2 in the MBR (set-up, see Figure 10).

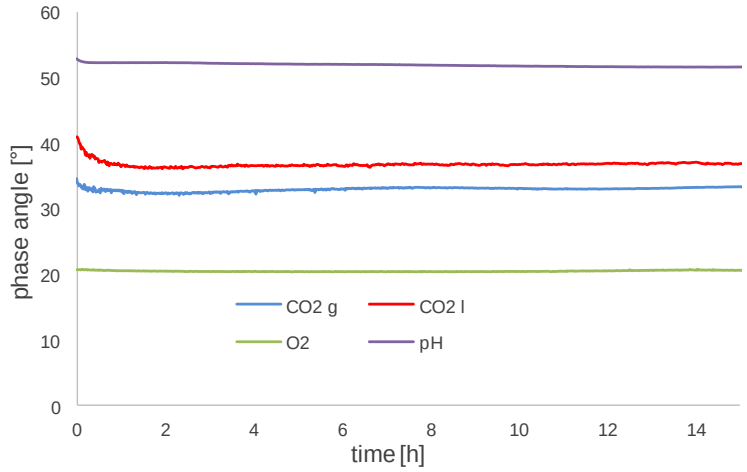

Figure 18: Equilibration of the sensor spots in the MBR over 15 h at 5 % CO_2 and 37 °C.

All sensor spots showed stable signals over the assumed measurement period using the measurement set-up. While the O_2 and pH sensor were immediately stable, the CO_2 sensors needed an equilibration phase of around 1 – 3 h , as already shown for the sensor foils (Figure 12, Figure 13, Figure 14). As a consequence, the sensors have a reasonable stability for a short application (equilibration, calibration and cultivation) within 24 h. Hence, equilibration was done before the first use of the sensor and then the sensors were used in a continuous manner, where a calibration was done directly before starting a new cultivation.

3.2.1.2 Shelf life

Shelf life could only be roughly estimated, since there were no long term storage tests done so far. After preparation of the sensors they were stored in the dark, at 4 °C under CO_2 atmosphere until application in the MBR. This avoids damage, such as photobleaching and poisoning of the sensors. [17][20] Before storage of the sensors at 4 °C they were intermediately stored at RT for two days. For the tests different sensor plates were used and they were exchanged after a few measurements. With all sensors, similar results were obtained. Measured phase angles ranged from around 50° to 30° with varying CO_2 concentrations from 1.5 to 25 %. In conclusion, storage of the sensor spots for at least two

months does not influence the function of the sensors. All sensors for CO_2, pH and O_2 showed stable signals and responded to changes of the measurement parameter. Fritzsche *et al*. found that shelf life mainly depends on the used polymer for the protective layer. PDMS was regarded to have rather poor protective properties due to high permeability for acidic gases such as H_2S. [17][46] Under ambient conditions the sensor with PDMS was completely poisoned after 1.5 months, while stability was remained when using Hyflon AD 60. [17] Hence it can be assumed that shelf life of the prepared CO_2 sensors can exceed two months as long as poisoning is prevented by appropriate storage conditions.

3.2.1.3 Operational stability

Further, the operational stability of the sensors was estimated. As already discussed there is a drift in the sensor signal, so it was only checked whether they respond to changes in CO_2 concentration even if the phase angles vary from one measurement to the other. Two kinds of investigations were done to estimate the operational stability.

On the one hand, an unused sensor plate was integrated into the MBR and continuous measurements were performed over one week by altering calibration and cultivation. Here the CO_2 sensors showed a high drift in the signal, but they still responded to changes in the measurement parameters and hence can be used for at least one week of continuous measurements. This will be discussed in correlation with the reproducibility of the sensors (see Figure 21, chapter 3.2.3).

On the other hand, reuse of the sensors after altering measurement and storage was investigated. For that the functionality of one sensor plate was tested by calibration in NaCl solution (0.9 wt%) at RT, after different periods of storage. Following the sensor preparation and in between measurements, the sensor plate was stored at 4 °C under CO_2 atmosphere in the dark. Figure 19 shows the measured calibration results.

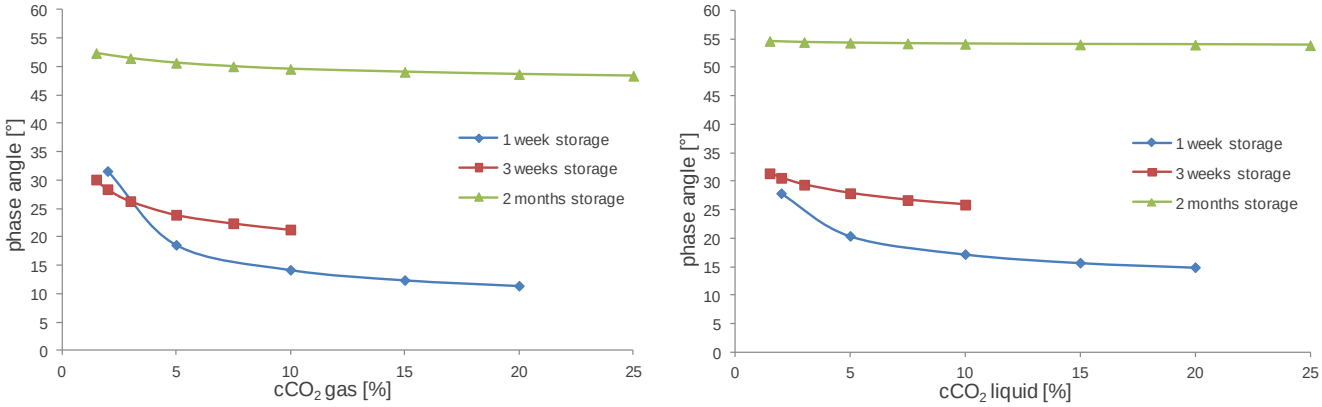

Figure 19: Comparison of the performance of one sensor plate over time in gaseous (left) and liquid (right) phase. Tests were performed ~ one week after sensor preparation, ~3 weeks after sensor preparation and ~ 2 months after sensor preparation; at RT, in NaCl solution between 1.5 and 25 % CO_2.

Table 11 lists the differences between the phase angles in low CO_2 concentrations to estimate the sensitivity after different periods of storage.

Table 11: Measured difference of the phase angles between 1.5 or 2 % and 5 % CO_2 in gas and liquid phase over time.

storage time	concentration difference [%]	$\Delta\varphi_{Gas\ phase}$ [°]	$\Delta\varphi_{Liquid\ phase}$ [°]
one week	2 – 5	13	7.5
three weeks	2 – 5	4.5	2.7
two month	1.5 – 5	1.72	0.32

Calibration was first done one week after sensor preparation. Three weeks of storage later, the calibration was repeated with the result that the sensor still responded to variation of CO_2 concentrations. Although the phase angles increased slightly and sensitivity decreased, the response was still in a range where it could be used for the application in the MBR. After two months a 3rd measurement was done, where the phase angles increased drastically and sensitivity decreased. In liquid phase the difference between 1.5 and 25 % was less than 1 ° and hence after two months of discontinuous use an application as CO_2 sensor is not possible anymore.

In general phase angles increased and differences of phase angles by changing CO_2 concentrations decreased over time. This shows a loss of sensitivity over time. The loss of stability and decrease in sensitivity might be explained by bleaching, leaching or poisoning of the sensor. [8][9][17][47] Further, the sensors might dry out due to loss of water and degradation of the base, which decreases the sensor stability. [15][25][52]

3.2.2 Sensitivity

Besides stability measurements, the sensitivity and the dynamic range of the CO_2 sensors was investigated. This was done by calibration of the sensors in KPi buffer (0.1 M, pH 7.4) at different CO_2 concentrations in the MBR. Two different measurements were performed. On the one hand, the concentration range from 1.5 % to 10 % CO_2 was tested to investigate sensitivity at low concentrations. On the other hand, the highest measurable concentration was checked by measuring phase angles between 1.5 % and 25 % CO_2 (Figure 20). Concentrations lower than 1.5 % were not measured since this was not possible with the used MFCs (as described in chapter 2.4.3).

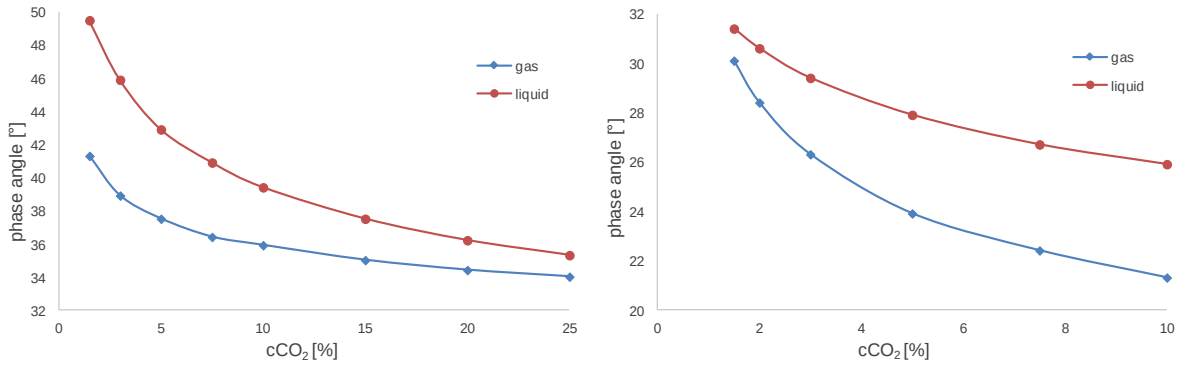

Figure 20: Comparison of two calibration curves of the CO_2 sensors spots in gas and liquid phase in different concentration ranges. Left: calibration from 1.5 to 25 % to estimate highest possible concentration. Right: calibration from 1.5 to 10 % to estimate phase shift at low concentrations and the possibility to distinguish small concentration differences.

As already expected at low concentrations small differences can be detected. This was already shown for several sensors, where the lower concentration range of the calibration always shows higher sensitivity. [11][12][15]–[18] In the range from 1.5 to 2 % the difference in phase angle was 1.7° in gas and 0.8° in liquid phase, respectively, whereas the difference between 7.5 and 10 % was only 1.1° in gas phase and again 0.8° in liquid phase, respectively (Figure 20; right). Further, measurements up to 25 % CO_2 were possible. Since it was not expected that CO_2 concentrations in the bioreactor exceed 15 % [23a], the measurable concentration range is suitable for cultivations in the MBR. Compared to other CO_2 sensors this range also seems to be reasonable. Commercial optical CO_2 sensors from PreSens are available for a concentration range from 1 – 25 %. [45] Furthermore, there are various different CO_2 sensors described in the literature, where the measurement range depends on the used dye and sensor composition. There are sensors available for trace concentrations below

1 %, [17] many sensors show a good dynamic range up to 10 – 30 % [15][18][25][26] and there exist also sensors that can measure up to 100 % CO_2. [18]

Moreover, strong differences between the single sensors were observed. The measured phase angles between 1.5 and 10 % were in the range of 50 – 35° for the one sensor (Figure 20, left) and 32 – 22° (Figure 20, right) for the other. However, regarding the differences of the phase angles in liquid and gas phase, it seems that both sensors show good performance. Regarding concentrations between 1.5 and 10 %, the left sensor showed a difference of ~5° and ~10° for gas and liquid phase, respectively. The right sensor showed differences of the phase angle of ~9° and ~5.5° in gas and liquid phase, respectively. These results demonstrate the necessity of a calibration for each single sensor.

3.2.3 Reproducibility

Further, it was tested if a stable and reproducible calibration is possible with the CO_2 sensors. For that calibration was done in liquid (KPi buffer, 0.1 M pH 7.4) and gas phase at 37 °C after equilibration of the sensors. The sensors were calibrated three times within one week and after each calibration, cultivation with *S. carnosus* was done (Figure 21).

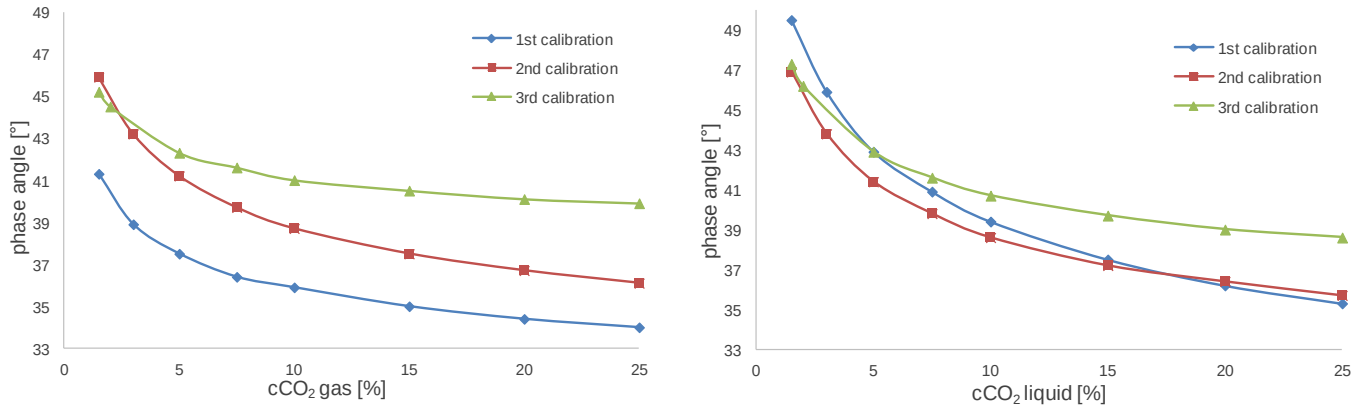

Figure 21: Comparison of three calibration curves done at the same conditions, at 37 °C, with unchanged set-up and the same sensor plate. Calibrations were done within one week and after each calibration one cultivation with *S. carnosus* was done. Left: calibration of the gas phase. Right: calibration in KPi buffer (pH 7.4, 0.1 M). First calibration was done after equilibration, second calibration after first cultivation, third calibration after second cultivation.

Comparing the calibrations, there are strong differences between the single measurements. The hyperbolic trend was maintained; however, the sensitivity, especially at high concentrations, became lower over time. Further, the phase angle increased with time as already discussed regarding the operational stability (chapter 3.2.1.3). Additionally, the sensors needed again some time for equilibration (~ 2 – 3 h) after each cultivation. This might

be due to the changing media (from LB media with living cultures to sterile KPi buffer). As already discussed in chapter 3.1.2 an equilibration time was needed upon changing from storage conditions to measurement conditions. This might be explained by variation of humidity, resulting in changes of the measurement signal. [15][20] On the other hand, the sensors might be influenced by the growing cultures. *S. carnosus* is known to produce lactate from glucose [37][53][54], which probably affects the sensor performance. This might also explains the strong variations in the calibration curves. The sensor might be poisoned due to media components produced during cultivation. To ensure a reliable calibration the sensors were calibrated prior to each cultivation.

The same test (Figure 21) was performed with cultivation of *S. cerevisiae* at 30 °C (Figure **22**). Again three calibrations were carried out and cultivation of *S. cerevisiae* was done in between.

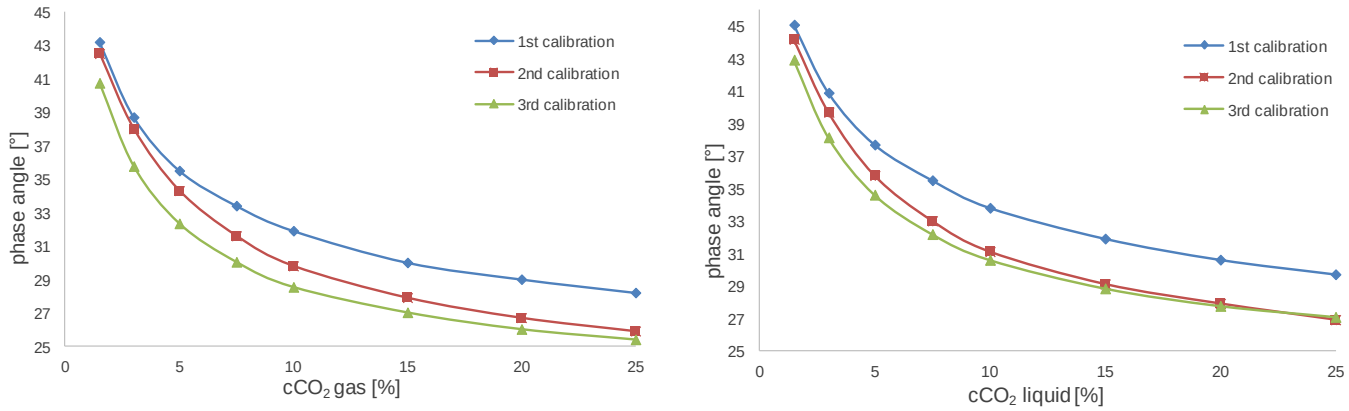

Figure 22: Comparison of three calibration curves done at the same conditions, at 30 °C, with unchanged set-up and the same sensor plate. Calibrations were done within one week and after each calibration one cultivation with *S. cerevisiae* was done. Left: calibration of the gas phase. Right: calibration in KPi buffer (pH 7.4, 0.1 M). First calibration was done after equilibration, second calibration after first cultivation, third calibration after second cultivation.

Other than at 37 °C, the sensors were more stable and gave rather reproducible data, also the hyperbolic trend in all curves was very similar. Here, the phase angle decreased from the first to the last calibration, which might be due to poisoning of the sensor. [17] However, the second and third calibrations were very similar with little changes in phase shift (< 2° at low CO_2 concentrations and < 0.5° at high concentrations). The better reproducibility might be due to higher sensor stability with the used media and culture. However, also the temperature could have a large influence. Since the temperature affects the sensitivity, it is not astonishing if also the stability is influenced by the measurement temperature and that lower temperatures lead to an increased stability. Moreover, there was no additional need for an equilibration

phase after a cultivation performed at 30 °C, which supports the assumption of an enhanced stability at 30 °C.

3.2.4 Dependence on reaction media

Calibrations were done in KPi buffer (0.1 M, pH 7.4) at 37 °C, while LB-media was used for cultivation. Calibrations were not done in LB media since there is a high probability of bacterial growth under these conditions which could lead to changes in pH, O_2 and CO_2 concentrations during calibration.

Therefore, it was investigated if the signal changes significantly when different media are used. The applied sensor was equilibrated at 5 % CO_2, since in that range there is still high sensitivity. The influence of pH and ionic strength was tested with water, KPi buffer (0.1 M) at pH 4.5, 6.8 and 8.6, NaCl solution (150 mM) and LB media.

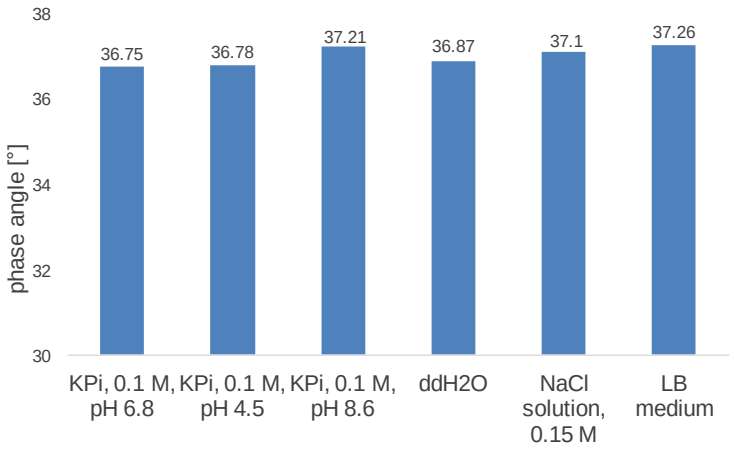

Figure 23: Dependence of the CO_2 sensor signal on different media, pH and ionic strength. Tests were done with the same sensor plate in equilibrium at 5 % CO_2 and 37 °C with H_2O, KPi buffer (0.1 M; pH 4.5, 6.8 and 8.6), NaCl solution (0.15 M) and LB media.

Figure 23 shows the dependency of the CO_2 signal on reaction media. The highest difference was 0.5°, which indicates a low dependency of the sensor signals on pH and ionic strength. Hence, it was concluded that the influence of the different reaction media on calibration is negligible, especially when regarding the comparably higher sensor drift over time.

3.3 Application of O_2, CO_2 and pH sensors in microbioreactor

The aim of the study was an application of the developed CO_2 sensors combined with O_2 and pH sensors in the MBR. The sensors should be used for characterization of fermentation of *S. carnosus* and *S. cerevisiae.* The development of CO_2 and O_2 concentration, pH and OD_{600} were measured during cultivation. The MBR as described in chapter 2.4.2 was used for several batch fermentations. Since the challenges regarding the CO_2 sensor were already discussed in chapter 3.2 here the focus will lie on the reactor set-up and fermentations. Challenges as well as the results from successful cultivations of *S. carnosus* and *S. cerevisiae* will be discussed.

3.3.1 Reactor design and application

The developed MBR was a 3D-printed device, composed of six different parts (Figure 9) made up of polyacrylate. The different parts were fixed by screws and magnets in order to obtain a tight system. Polyacrylate is a rather soft and elastic material [55] resulting in the bending of the material over time. Furthermore, the material is sensitive to EtOH and gets brittle if it was used for cleaning. Thus the use of EtOH was avoided and the MBR was cleaned with water and soap. After multiple uses, it was getting more challenging to tighten the reactor, due to deformation of the reactor parts.

Several trials of cultivation did not work out since the cultivation media dissipated over night. It was assumed that this happened due to leakage, but might also be caused by evaporation due to heating and aeration. Especially when 500 µL reaction volume were used, cultivations were not successful. For that reason air was humidified and 1 mL culture broth was used to prevent loss of reaction media due to evaporation. Tightness of the reactor was checked before starting the fermentations, but it was not always ensured over night. An exchange of the reactor is supposed after a few weeks of operation due to deformation of the material.

Moreover, there was a strong oxygen limitation during fermentation (Figure 24, Figure 26). Hence the aeration rate was increased to 15 mL/min, since a higher aeration rate improves the k_La. [33a] Unfortunately, fermentations at these conditions were not successful. There were two different scenarios observed. On the one hand, emptying of the MBR was observed, due to above mentioned reasons. On the other hand, even when the MBR was tight, there was still

no growth of the culture, indicating that sheer rates due to aeration were too high and damaged the cells. [33b]

Despite these challenges, two successful cultivations of *S. carnosus* and one of *S. cerevisiae*, including quantification of O_2, CO_2, pH and OD_{600}, could be carried out.

3.3.2 Cultivation of S. carnosus

First, cultivation of *S. carnosus* was tested and repeated several times. Figure 24 and Figure **25** show the two successful cultivations including quantification of O_2, CO_2 and pH. Both cultivations show a similar trend, however, production of CO_2 and depletion of O_2 differed as well as the cell growth. This is probably due to the use of a different media, where one contained 1.7 g/L glucose and the other 1 g/L glucose. Especially the biomass concentration (OD_{600}) is affected by the glucose concentration. [37]

Although the achieved OD_{600} and the time course of the cultivations were quite different with 1 g/L and 1.7 g/L glucose, the trend was similar. At the start of exponential growth, the oxygen concentration decreased, finally leading to an oxygen limitation. This was probably due to insufficient aeration. Jana Krull shows in her master thesis that cultivation of *S. carnosus* is possible without any oxygen limitation in a cuvette MBR. [37] Improvement of the oxygen supply might be achieved by higher aeration rates, aeration with smaller gas bubbles or use of pure oxygen instead of air. [33a] Shortly before the O_2 concentration went to zero, the maximum of CO_2 was reached. This was expected since the microbial consumption of glucose requires oxygen and produces CO_2 according to equ. 32. [56a]

$$C_6H_{12}O_6 + 6O_2 \rightarrow 6CO_2 + 6H_2O \qquad \text{equ.32}$$

Further the pH showed a minimum approximately at the maximum of CO_2 concentration. The decrease of pH during cultivation can probably be explained by production of lactic acid. [37][53][54] When growth reached the stationary phase, the O_2 and CO_2 concentrations approximated their starting values, while the pH increased. Increasing O_2 and decreasing CO_2 concentrations as well as increase in pH might be a result of depletion of glucose. [37][54]

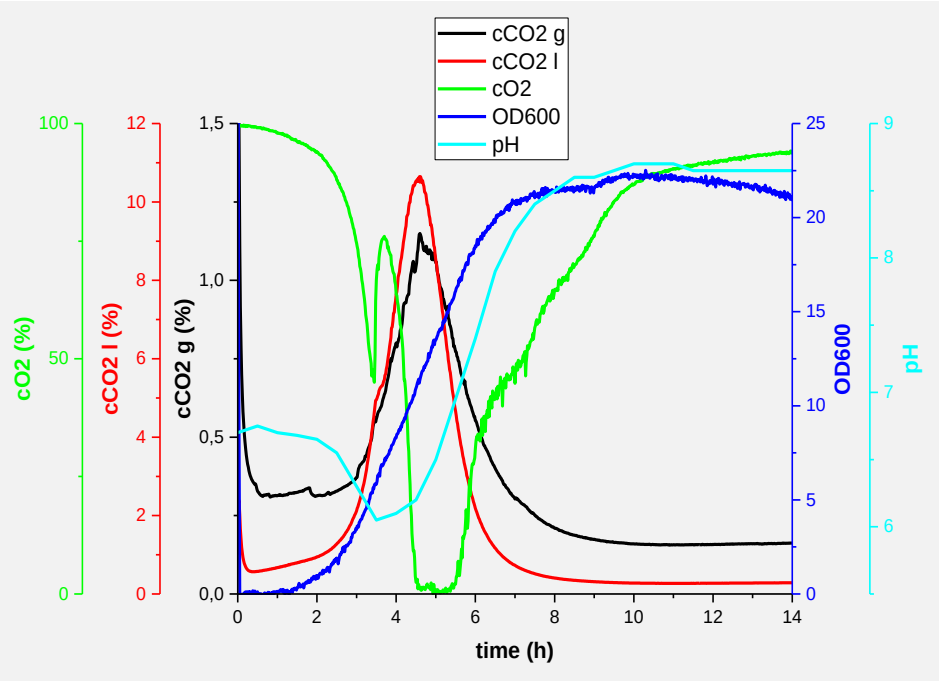

Figure 24: Cultivation of *S. carnosus* at 37 °C in the MBR. Development of OD_{600}, cCO_2 (gas and liquid), cO_2 and pH over culture time. Cultivation in LB media with 1.7 g/L glucose.

Figure 24 shows the cultivation of *S. carnosus* using 1.7 g/L glucose. At 4.5 – 5.5 h a strong oxygen limitation occurred correlating with the exponential growth phase. When bacterial growth became stationary, the oxygen concentration increased again and reached around 90 % after 14 h. The final OD_{600} was around 22. Also after approximately 4.5 h, when oxygen became limiting, the CO_2 concentration was the highest. In liquid phase a concentration of around 10 % was reached, while in gas phase only 1.5 % CO_2 were produced. At the end of the cultivation the CO_2 concentration approached again 0 % and the O_2 concentration reached again almost 100 %. The lowest pH was around 6 which was also reached after around 5.5 h when CO_2 concentration showed a maximum. At the end of the exponential phase the pH increased to 8.5. These values correspond well with the pH observed in the cuvette MBR from Jana Krull, where maximum pH was 8 and the minimum at 6. [37]

At 4 h there was a peak in the oxygen curve, where the oxygen level increased for a short time. At the same point the slope of the growth curve changed slightly and also in the dissolved CO_2 a deceleration of CO_2 production was observed for a short time. This might be a hint of changes in metabolic activities. At that point glucose might have been fully or mainly converted to lactic acid, which was then further used as substrate for culture growth. [37]

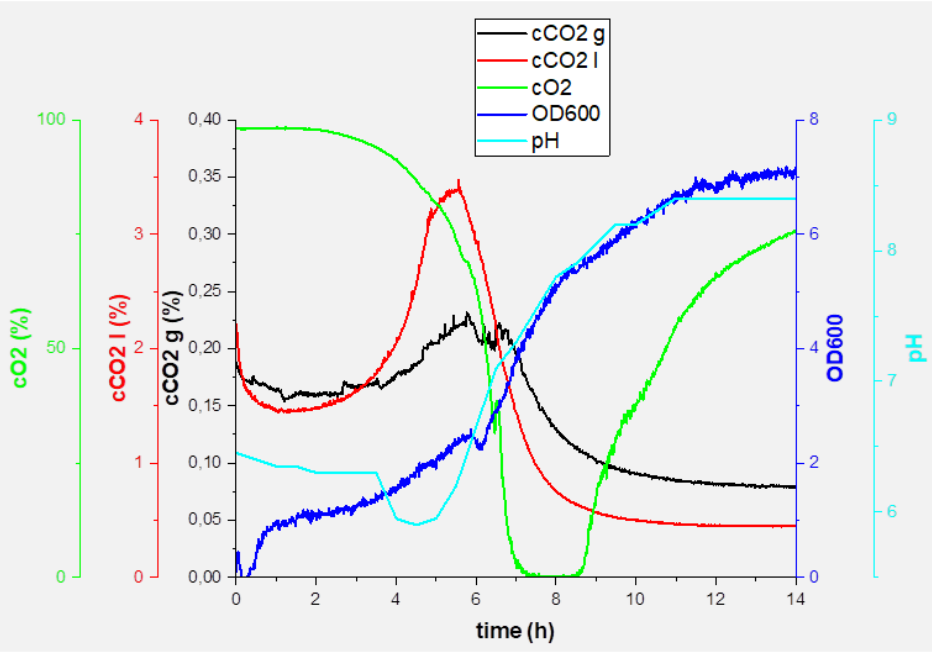

Figure 25: Cultivation of *S. carnosus* at 37 °C in the MBR. Development of OD_{600}, cCO_2 (gas and liquid), cO_2 and pH over culture time. Cultivation in LB media with 1 g/L glucose.

The second culture (Figure 25) was done with freshly prepared media and therefore with only 1 g/L glucose. Glucose concentration was lowered in order to prevent strong oxygen limitation. The reached limits and concentrations were clearly different; however, the trend was the same as for the first cultivation (Figure 24). Oxygen limitation started after around 7 h until 8.5 h. The maximal CO_2 concentration was already reached at ~6 h. Again CO_2 concentration in liquid phase was around 10 times higher than in the gas phase (3.5 and 0.2 %, respectively). The lowest pH was around 6 and observed at 5 – 6 h. The lower values of produced CO_2 correspond to a decrease in growth rate. The maximal OD_{600} was 7 and can be explained by the lower initial glucose concentration. [37] Again at around 6.5 h a small peak in the oxygen curve was observed, which correlates to a change in growth (as described with the first culture, Figure 24).

As already described in chapter 3.2, the CO_2 sensors show a strong signal drift. Therefore, calibrations were performed directly before starting the cultivation to ensure as accurate values as possible. Further, calibration of concentrations below 1.5 % was not possible with the given set-up. Due to the above mentioned challenges it has to be kept in mind that the determined values can only be a rough estimation of the concentration range. For an intensive quantification further effort has to be done in sensor as well as in reactor design.

3.3.3 Cultivation of S. cerevisiae

Figure 26 shows a cultivation of *S. cerevisiae* done in the MBR.

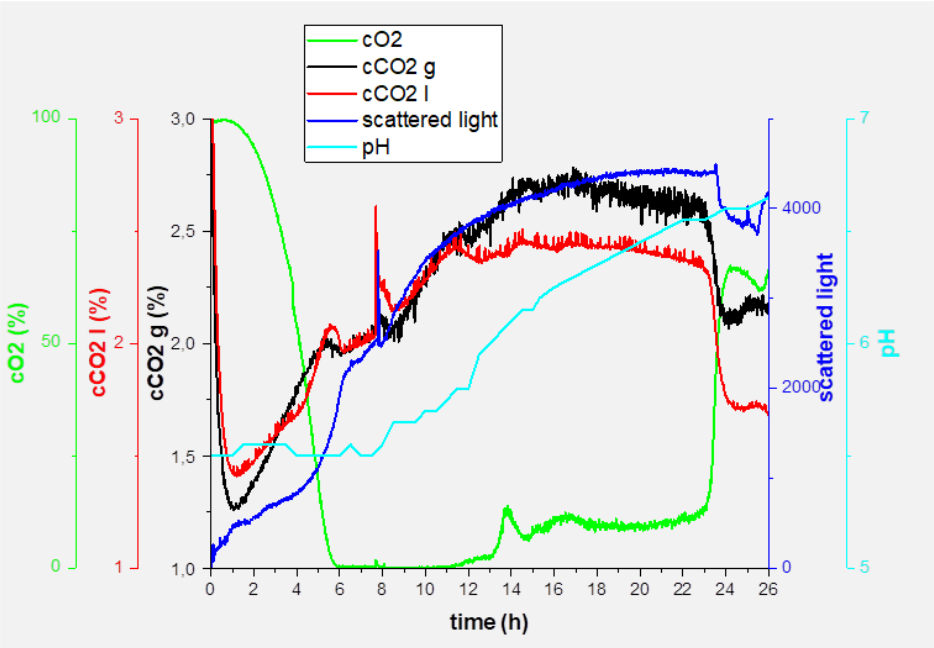

Figure 26: Cultivation of *S. cerevisiae* at 30 °C in the MBR. Development of scattered light, cCO_2 (gas and liquid), cO_2 and pH over cultivation time. Cultivation in LB complex media, 7.5 g/L glucose.

During cultivation of *S. cerevisiae* a strong oxygen limitation was observed between 6 and 22 h. Then the O_2 concentration increased again, but only reached a value of around 70 % at the end. Growth approached an exponential phase between 4 and 10 h and then slowly switched to a stationary phase. In this case no correlation between scattered light and OD_{600} was done. However, OD_{600} at the end of cultivation was 0.7, while the OD_{600} in the shaking flask was 1.2. The high difference in OD_{600} for the shaking flask and the MBR is probably due to the strong oxygen limitation. Reasons for the oxygen limitation are again too big gas bubbles and too low aeration rates. [33a] The produced CO_2 in liquid and gas phase was very similar, reaching a maximum of 2.5 % between 10 – 22 h, corresponding to the oxygen limitation. Similar trends were observed by Anderlei *et al.*, where the oxygen decreased constantly within the first 8 hours and finally became limiting. At the same time the CO_2 production rate increased, reaching a maximum shortly before complete oxygen limitation. Within this first hours glucose was consumed and EtOH produced, followed by consumption of EtOH. [57] The pH was constant at around 5.5 over the first 8 h and then increased constantly up to 6.5. Since no acids were expected to be formed during cultivation it is reasonable that the pH remains rather constant.

This shows that cultivation of *S. cerevisiae* is in principle possible with the used set-up and also the sensors can be used for different cultivations. As shown in Figure 22, chapter 3.2.3, the CO_2 sensors are more stable at 30 °C and hence application of the sensors is more reasonable under these conditions. However, here the main challenge is to overcome the oxygen limitation and to ensure an exponential growth of the cells. Hence before continuing with cultivations, efforts in reactor design are necessary. Since increasing the aeration rate is not possible without cell damage, it is necessary to either change the design of the reactor in order to decrease the bubble size or to aerate with pure oxygen. [33a]

4 Conclusion

In this study a CO_2 sensor was developed and characterized for an application in a MBR.

An emulsion based system was used for development of the CO_2 sensor and different compositions were tested. It was found that sensors based on DMS without dilution showed the best results with regard to drifts and stability. After a rough testing of the produced sensor foils, miniaturization and production of functional CO_2 sensor spots succeeded. These sensor spots were characterized regarding sensitivity, stability, media and temperature dependence.

The sensors respond to CO_2 concentrations up to 25 % in liquid and gas phase with high sensitivity at low CO_2 levels and reasonable response times below 1 min. Sensor drifts were observed during calibrations and stability tests, however, stable signals were obtained for the measurement period used for the cultivations. It was concluded that calibration is necessary prior to each new cultivation. However, the sensors can be used for at least one week of continuous measurement. Moreover, the sensors can be stored over 2 months without loss of function and discontinuous use is possible for a few weeks, before the sensors become insensitive to changes in CO_2 concentrations. Additionally, there is little dependence of the sensor performance on the used media, which facilitates the calibration. Regarding the measurement temperature, temperature dependence was assumed, but no trend was observed. However, stability and reproducibility are increased at lower temperatures.

The produced CO_2 sensors for gas and liquid phase as well as sensors for pH and O_2 measurements were integrated into a MBR and cultivation of *S. cerevisiae* and *S. carnosus* were investigated. Application of the sensors was successful for on-line monitoring of pH, cO_2, cCO_2 as well as OD_{600}. Although all sensors worked in the MBR, challenges in the reactor design concerning strong oxygen limitations, as well as leaking or evaporation of the media during the cultivation were observed.

To summarize, successful application of the sensors in the MBR was possible. However, calibration and sensor stability remain challenging as well as oxygen supply. For future applications further attempts in sensor development and reactor design might be necessary.

5 Abbreviations

Table 12: Abbreviations used in this work.

Abbreviation	Full name
azaBODIPY	BF2-chelated tetraarylazadipyrromethane dyes
Catalyst	Platinum(0)-1,3-divinyl-1,1,3,3-tetramethyldisiloxane complex
CF	conversion factor for CO_2 gas flow
Copolymer	(25-35 % Methylhydroxysiloxane) dimethylsiloxane copolymer
DLR	dual lifetime referencing
DMS	Dimethylsiloxane-ethyleneoxide block copolymer (25% non-siloxane)
EB	Egyptian Blue
EtOH	Ethanol
FOCS	Fibre optic chemical sensor
HMS	Hexamethyldisiloxane
HTPS	Hydroxypyrene trisulfonic acid
KPi buffer	Potassium phosphate buffer
MBR	Microbioreactor
MFC	Mass flow controller
OD600	Optical density at 600 nm
PDMS	Polydimethylsiloxane
PET	Photoinduced electron transfer
PMMA	Polymethylmethacrylat
Polymerisation retardant	1,3,5,7-Tetravinyl-1,3,5,7-tetramethylcyclotetrasiloxane
PS	Polystyrol
PtTPTBPF	Platinum(II)-meso-tetra(4-fluorophenyl) tetrabenzoporphyrin
RET	Resonance energy transfer
RT	Room temperature
SNARF	Seminaphthorhodafluors

6 Literature

[1] B. Valeur, *Molecular Fluorescence Principles and Applications*. WILEY-VCH Verlag GmbH: Weinheim, 2001; a) 8ff, b)90ff, c) 54, d) 42, e) 48ff, f) 133ff.

[2] J. R. Lakowicz, *Principles of fluorescence spectroscopy*, 3rd ed. Springer: New York, 2006; a)1-11, b)336ff, c) 13ff, d) 27ff, e) 97ff.

[3] T. Jokic, S. M. Borisov, R. Saf, D. A. Nielsen, M. Kühl, and I. Klimant, "Highly photostable near-infrared fluorescent pH indicators and sensors based on BF2-chelated tetraarylazadipyrromethene dyes," *Anal. Chem.* **2012**, 84, 6723–6730,.

[4] M. Strobl, T. Rappitsch, S. M. Borisov, T. Mayr, and I. Klimant, "NIR-emitting aza-BODIPY dyes-new building blocks for broad-range optical pH sensors," *Analyst*, vol. **2015**, 140, 7150–7153,.

[5] R. Narayanaswamy, "Optical Chemical Sensors: Tranduction and Signal processing," *Analyst* **1993**, 118, 317–322,.

[6] C. McDonagh, C. S. Burke, and B. D. MacCraith, "Optical Chemical Sensors," *Chem. Rev.* **2008**, 108, 400–422,.

[7] R. Kellner, J.-M. Mermert, M. Otto, M. Valcárcel, and H. M. Widmer, *Analytical Chemistry*, 2nd ed. WILEY-VCH Verlag GmbH: Weinheim, 2004; a) 1067ff.

[8] C. Huber, I. Klimant, C. Krause, and O. S. Wolfbeis, "Dual lifetime referencing as applied to a chloride optical sensor," *Anal. Chem.* **2001**, 73, 2097–2103.

[9] G. Liebsch, I. Klimant, C. Krause, and O. S. Wolfbeis, "Fluorescent imaging of pH with optical sensors using time domain dual lifetime referencing," *Anal. Chem.* **2001,** 73, 4354–4363.

[10] Hulanicki, A.; Glab, S.; Ingman, F, "Chemical Sensors Definition and Classification," *Pure Appl. Chem.* **1991**, 63, 1247–1250.

[11] F.-G. Banica, *Chemical Sensors and Biosensors Fundamentals and Applications*, John Wiley & Sons Ltd: Chichester, 2012; a) 1, b) 435ff.

[12] B. R. Eggins, *Chemical Sensors and Biosensors*. John-Wiley & Sons Inc: Hoboken,

2002; a) 4, b) 7.

[13] P. Gruber, M. P. C. Marques, N. Szita, and T. Mayr, “Integration and application of optical chemical sensors in microbioreactors,” *Lab Chip* **2017,** 17, 2693–2712.

[14] L. Tolosa, Y. Kostov, and G. Rao, “Fluorescence-based Sensors for Bioprocess Monitoring,” in *Fluorescence Sensors and Biosensors*, Taylor & Francis Group: Abingdon, 2006, 333–349.

[15] A. Mills, Q. Chang, and N. McMurray, “Equilibrium Studies on Colorimetric Plastic Film Sensors for Carbon Dioxide,” *Anal. Chem.* **1992**, 64, 1383–1389.

[16] C. S. Chu, Y. L. Lo, and T. W. Sung, “Review on recent developments of fluorescent oxygen and carbon dioxide optical fiber sensors,” *Photonic Sensors* **2011**, 1, 234–250.

[17] E. Fritzsche, P. Gruber, S. Schutting, J. P. Fischer, M. Strobl, J. D. Müller, S. M. Borisov, and I. Klimant, “Highly sensitive poisoning-resistant optical carbon dioxide sensors for environmental monitoring,” *Anal. Methods* **2017**, 9, 55–65.

[18] S. Schutting, T. Jokic, M. Strobl, S. M. Borisov, D. De Beer, and I. Klimant, “NIR optical carbon dioxide sensors based on highly photostable dihydroxy-aza-BODIPY dyes,” *J. Mater. Chem. C* **2015**, 3, 5474–5483.

[19] X. Ge, Y. Kostov, and G. Rao, “Low-cost noninvasive optical CO2 sensing system for fermentation and cell culture,” *Biotechnol. Bioeng.* **2005**, 89, 329–334.

[20] A. Eaton and K. Mills, “Optical sensors for carbon dioxide: An overview of sensing strategies past and present,” *Qimica Anal.* **2000**, 19, 75–86.

[21] E. Riedel, *Allgemeine und anorganische Chemie*, 6th ed. Walter de Gruyter: Berlin, 1994; a)267.

[22] G. Hengge, *Anorganische Chemie*, 5th ed. VCH: Weinheim, 1990, a) 305.

[23] W.-S. Hu, *Cell culture bioprocess engineering*, 1st ed. Wei-Shou Hu, 2013; a) 218ff, b) 281ff.

[24] G. Rao, *Optical Sensor Systems in Biotechnology*. Springer-Verlag: Berlin Heidelberg, 2009; a) 24.

[25] A. Mills and L. Monaf, “Thin plastic film colorimetric sensors for carbon dioxide: Effect of plasticizer on response,” *Analyst* **1996**, 121, 535–540.

[26] J. Sipior, S. Bambot, M. Romauld, G.M. Carter, J. Lakowicz, G. Rao, “A lifetime-based optical CO2 gas sensor with blue or red excitation and stokes or anti-stokes detection” *Anal. Biochem.* **1995**, 227, 309–318.

[27] J. Severinghaus and A. Freeman, “Electrodes for Blood pO2, and pCO2, Determination,” *J. Appl. Physiol.* **1958**, 13, 515–520.

[28] R. Krull, S. Lladó-Maldonado, T. Lorenz, S. Büttgenbach, and S. Demming, “Microbioreactors,” in *Microsystems for Pharmatechnology: Manipulation of Fluids, Particles, Droplets, and Cells.*, Springer: Berlin Heidelberg, 2016, pp. 99–152.

[29] H. M. Hegab, A. ElMekawy, and T. Stakenborg, “Review of microfluidic microbioreactor technology for high-throughput submerged microbiological cultivation,” *Biomicrofluidics* **2013**, 7, 1–14.

[30] S. Kumar, C. Wittmann, and E. Heinzle, “Minibioreactors,” *Biotechnol Lett* **2004**, 26, 1–10.

[31] N. Szita, A. Zanzotto, P. Boccazzi, A. J. Sinskey, M. A. Schmidt, and K. F. Jensen, “Monitoring of cell growth, oxygen and pH in microfermentors.,” in *In Micro Total Analysis Systems*, Springer Netherlands, 2002, pp. 7–9.

[32] M. Leester-Schädel, T. Lorenz, F. Jürgens, and C. Richter, “Fabrication of Microfluidic Devices,” in *Microsystems for Pharmatechnology: Manipulation of Fluids, Particles, Droplets, and Cells.*, Springer: Berlin Heidelberg, 2016, pp. 23–58.

[33] P. D. Doran, *Bioprocess Engineering Principles*, 2nd ed. Academic Press: Oxford, 2013; a) 393ff; b)315ff.

[34] S. M. Borisov, C. Würth, U. Resch-Genger, and I. Klimant, “New life of ancient pigments: Application in high-performance optical sensing materials,” *Anal. Chem.* **2013**, 85, 9371–9377.

[35] B. Nacht, C. Larndorfer, S. Sax, S. M. Borisov, M. Hajnsek, F. Sinner, E. J. W. List-Kratochvil, and I. Klimant, “Integrated catheter system for continuous glucose

measurement and simultaneous insulin infusion," *Biosens. Bioelectron.* **2014**, 64, 102–110.

[36] P. Sulzer, "Utilization of microdispensing technology for the application of optical sensors," Master's thesis, Graz University of Technology, 2016.

[37] J. Krull, "Cultivation of Staphylococcus carnosus at micro-scale - Influence of different reactor performances," Master's thesis, Technische Universität Braunschweig, 2017.

[38] C. Hönnscheidt, "Entwicklung kolloiddisperser Wirkstoffformulierungen auf Basis von Biopolymeren," Dissertation, Technische Universität Braunschweig, 2016.

[39] "D4 Hydromed." http://www.advbiomaterials.com/products/hydrophilic/hydromed.html. [Accessed: 27-Oct-2018].

[40] J. Wang, Z. Wen, B. Yang, and X. Yang, "Optical carbon dioxide sensor based on fluorescent capillary array," *Results Phys.* **2017**, 7, 323–326.

[41] "DMS." https://www.chemicalbook.com/ChemicalProductProperty_DE_CB0344825.htm. [Accessed: 27-Oct-2018].

[42] H. W. Haesslin, H. F. Eicke, and G. Riess, "Dimethylsiloxane-ethylene oxide block copolymers, 1 - Microphase separation of low segment mass copolymers and their compatibility with water and oil," *Makromol. Chem.* **1984**, 185, 2625–2645.

[43] S. Schutting, S. M. Borisov, and I. Klimant, "Diketo-pyrrolo-pyrrole dyes as new colorimetric and fluorescent pH indicators for optical carbon dioxide sensors," *Anal. Chem.* **2013**, 85, 3271–3279.

[44] S. Schutting, I. Klimant, D. De Beer, and S. M. Borisov, "New highly fluorescent pH indicator for ratiometric RGB imaging of pCO2," *Methods Appl. Fluoresc.* **2014**, 2, 1-8.

[45] PreSens, "Optical CO 2 Sensors & Meters." https://www.presens.de/products/co2/sensors.html. [Accessed: 27-Oct-2018].

[46] J. C. Lötters, W. Olthuis, P. H. Veltink, and P. Bergveld, "The mechanical properties of

the rubber elastic polymer polydimethylsiloxane for sensor applications," *J. Micromechanics Microengineering* **1997**, 7, 145–147.

[47] C. Boniello, T. Mayr, J. M. Bolivar, and B. Nidetzky, "Dual-lifetime referencing (DLR): A powerful method for on-line measurement of internal pH in carrier-bound immobilized biocatalysts," *BMC Biotechnol.* **2012**, 12, 1–10.

[48] D. S. Carvalho, C. J. B. Joia, and O. R. Mattos, "Corrosion rate of iron and iron-chromium alloys in CO2 medium," *Corros. Sci.* **2005**, 47, 2974–2986.

[49] S. L. Wu, Z. D. Cui, F. He, Z. Q. Bai, S. L. Zhu, and X. J. Yang, "Characterization of the surface film formed from carbon dioxide corrosion on N80 steel," *Mater. Lett.* **2004**, 58, 1076–1081.

[50] W. R. Whitney, "The Corrosion of Iron.," *J. Am. Chem. Soc.* **1903**, 25, 394–406.

[51] D. A. López, T. Pérez, and S. N. Simison, "The influence of microstructure and chemical composition of carbon and low alloy steels in CO2 corrosion. A state-of-the-art appraisal," *Mater. Des.* **2003**, 24, 561–575.

[52] G. G. Vurek, P. J. Feustel, and J. W. Severinghaus, "A FIBER OPTIC PCO2 SENSOR," *Ann. Biomed. Eng.* **1983**, 11, 499–510.

[53] K. H. SCHLEIFER and U. FISCHER, "Description of a New Species of the Genus Staphylococcus: Staphylococcus carnosus," *Int. J. Syst. Bacteriol.* **1982**, 32, 153–156.

[54] S. Dilsen, W. Paul, D. Herforth, A. Sandgathe, J. Altenbach-Rehm, R. Freudl, C. Wandrey, and D. Weuster-Botz, "Evaluation of parallel operated small-scale bubble columns for microbial process development using Staphylococcus carnosus," *J. Biotechnol.* **2001**, 88, 77–84.

[55] "polyacrylates," *polymer database*. https://polymerdatabase.com/polymer classes/Polyacrylate type.html. [Accessed: 31-Oct-2018].

[56] W. Fritsche, *Mikrobiologie*, 1st ed. Gustav Fischer Verlag: Jena, 1990; a) 144.

[57] T. Anderlei, W. Zang, M. Papaspyrou, and J. Büchs, "Online respiration activity measurement (OTR, CTR, RQ) in shake flasks," *Biochem. Eng. J.* **2004**, 17, 187–194.

7 Tables and Figures

Figure 1: Jablonski diagram – one schematic form. S_0, S_1 and S_2: singlets in ground, first and second electronic state. T_1: first triplet state. 0, 1 and 2 indicate the vibrational energy levels of each state. [2a] 1

Figure 2: Scheme for oxidized electron transfer using PET. [1b] 3

Figure 3: RET – spectral overlap of absorption and emission spectrum. [2c] 6

Figure 4: Scheme of DLR. A: In absence of the analyte the indicator is in its unquenched state. B: Presence of the analyte which quenches the fluorescence signal of the indicator. The overall phase angle changes. [8] 10

Figure 5: MonoOH azaBODIPY for optical CO_2 sensing. 18

Figure 6: General set-up for characterization of the sensor foils. Tests were performed in liquid or gas phase, between 0 and 20 % CO_2 concentration. 1 measurement cell; 2 PICCOLOS; 3 gas washing bottles; 4 MFC 34

Figure 7: General set-up for measuring response times. In a Schott flask the buffer was saturated with CO_2 (5 or 15 %). The buffer was then manually pumped into a flow-through cell containing the sensor foil. 1 syringe; 2 Schott flask with buffer; 3 MFC; 4 flow through cell; 5 PICCOLO. 35

Figure 8: Sensorspots on polycarbonate substrate. pH, O_2 and CO_2 for measuring in liquid and gas phase. 36

Figure 9: Microbioreactor design: Different parts of the microreactor used for cultivation. 1 microreactor inner view, 1a connection for cooling water, 1b gas in/outlet; 2 microreactor front site; 3 sealing; 4 connector for filling; 5 backside of the reactor composed of a holder and the sensorplate; 6 reactor – back view – including sealing and sensorplate; 7 whole reactor with sensorplate and connector fixed into the docking station providing connection to the cooling system and glass fibres; 8 docking station – front view – stationary part for fixation of the reactor system; 9 docking station – back view – the docking station provides connections to the cooling system and enables positioning of the glass fibres and temperature sensor. 37

Tables and Figures

Figure 10: Measurement set-up for cultivation and calibration in the MBR. 1 Mass flow controller; 2 thermostat; 3 reactor with opaque cover; 4 Scott flask with water to humidify incoming gas; 5 pressure valve for regulation of the gas flow; 6 connections of cooling water to reactor; 7 glass fibres; 8 temperature control for the reactor; 9 LED for scattered light measurement; 10 Firesting; 11 Ocean optics; 12 controller to set mass flow. 38

Figure 11: Set-up for stability measurements of the sensor in liquid phase in the incubator (100 % humidity, 5 % CO_2, 37 °C). 44

Figure 12: Sensorfoil, PDMS:D4 (10:1), 250 mM $CsHCO_3$, 0.4 % monoOH, 10 % EB, dilution 2:1 (PDMS:HMS), 1 MIL, TiO_2, measured in Tris-buffer at 25 °C. Left: complete measurement; right: 7^{th} cycle. 46

Figure 13: Sensorfoil, PDMS:DMS (10:1), 250 mM $CsHCO_3$, 0.4 % monoOH, 10 % EB, 1 MIL, TiO_2, measured in Tris-buffer at RT. Left: complete measurement; right: third cycle. . 47

Figure 14: Sensorfoil, PDMS:DMS (10:1), 250 mM $CsHCO_3$, 0.4 % monoOH, 10 % EB, 1 MIL, TiO_2, measured in gas phase at RT. Left: complete measurement; right: third cycle. ... 48

Figure 15: Phase angles at different CO_2 concentrations (0 – 20 %) and temperatures measured in Tris-HCl (0.1 M, pH 7.4). 49

Figure 16: Comparison of response time of the sensorfoil in liquid and gas phase at RT and 37 °C as well as response time of a sensorspot in liquid phase at RT. PDMS:DMS (10:1), 250 mM $CsHCO_3$, 0.4 % monoOH, 10 % EB, 1 MIL, TiO_2, measured in Tris-buffer at RT. Changing CO_2 concentration from 5 to 15 %. 50

Figure 17: Investigation of long term stability of the CO_2 sensor in the gas phase (A) and water (B). Incubation of the sensors at 100 % humidity, 37 °C and 5 % CO_2. Continuous measurement over 8 days. 51

Figure 18: Equilibration of the sensor spots in the MBR over 15 h at 5 % CO_2 and 37 °C. .. 53

Figure 19: Comparison of the performance of one sensor plate over time in gaseous (left) and liquid (right) phase. Tests were performed ~ one week after sensor preparation, ~3 weeks after sensor preparation and ~ 2 months after sensor preparation; at RT, in NaCl solution between 1.5 and 25 % CO_2. 55

Tables and Figures

Figure 20: Comparison of two calibration curves of the CO_2 sensors spots in gas and liquid phase in different concentration ranges. Left: calibration from 1.5 to 25 % to estimate highest possible concentration. Right: calibration from 1.5 to 10 % to estimate phase shift at low concentrations and the possibility to distinguish small concentration differences. 56

Figure 21: Comparison of three calibration curves done at the same conditions, at 37 °C, with unchanged set-up and the same sensor plate. Calibrations were done within one week and after each calibration one cultivation with *S. carnosus* was done. Left: calibration of the gas phase. Right: calibration in KPi buffer (pH 7.4, 0.1 M). First calibration was done after equilibration, second calibration after first cultivation, third calibration after second cultivation. 57

Figure 22: Comparison of three calibration curves done at the same conditions, at 30 °C, with unchanged set-up and the same sensor plate. Calibrations were done within one week and after each calibration one cultivation with *S. cerevisiae* was done. Left: calibration of the gas phase. Right: calibration in KPi buffer (pH 7.4, 0.1 M). First calibration was done after equilibration, second calibration after first cultivation, third calibration after second cultivation. 58

Figure 23: Dependence of the CO_2 sensor signal on different media, pH and ionic strength. Tests were done with the same sensor plate in equilibrium at 5 % CO_2 and 37 °C with H_2O, KPi buffer (0.1 M; pH 4.5, 6.8 and 8.6), NaCl solution (0.15 M) and LB media. 59

Figure 24: Cultivation of *S. carnosus* at 37 °C in the MBR. Development of OD_{600}, cCO_2 (gas and liquid), cO_2 and pH over culture time. Cultivation in LB media with 1.7 g/L glucose. 62

Figure 25: Cultivation of *S. carnosus* at 37 °C in the MBR. Development of OD_{600}, cCO_2 (gas and liquid), cO_2 and pH over culture time. Cultivation in LB media with 1 g/L glucose. 63

Figure 26: Cultivation of *S. cerevisiae* at 30 °C in the MBR. Development of scattered light, cCO_2 (gas and liquid), cO_2 and pH over cultivation time. Cultivation in LB complex media, 7.5 g/L glucose. 64

Figure 27: Comparison of the performance of the sensor foils: PDMS:D4 (10:1), 0.4 % monoOH, 10 % EB, dilution 2:1 (PDMS:HMS) and variations in film thickness and $CsHCO_3$ concentration. Measurement at 37 °C, in Tris-HCl buffer (0.1 M, pH 7.4). A: 250 mM

$CsHCO_3$, 1 MIL, TiO_2; B: 150 mM $CsHCO_3$, 1 MIL, TiO_2; C: 250 mM $CsHCO_3$, 0.5 MIL, no TiO_2; D: 150 mM $CsHCO_3$, 0.5 MIL, no TiO_2. 78

Figure 28: Measurement of sensorfoil PDMS:D4 (10:1) 0.4 % monoOH, 10 % EB, no dilution, 1 MIL, TiO_2 and $CsHCO_3$ (50 µL stock solution) in the gas phase. 78

Figure 29: Comparison sensorfoils, PDMS:D4 (10:1), 250 mM $CsHCO_3$, 0.4 % monoOH, 10 % EB, 1 MIL, measured in ddH_2O at RT. A: diluted PDMS:HMS 2:1; B: undiluted..... 79

Figure 30: Response time measurement: Sensorfoil, PDMS:DMS (10:1), 250 mM $CsHCO_3$, 0.4 % monoOH, 10 % EB, 1 MIL, TiO_2, measured in Tris-buffer at RT. 79

Figure 31: Example of a calibration for CO_2, between 1.5 and 25 % at 37 °C in KPi buffer or gas phase. 79

Figure 32: Example of a calibration for pH_2, between 5.5 and 8.7 at 37 °C in KPi buffer..... 80

Table 1: Properties of monoOH azaBODIPY for pH sensing..... 19

Table 2: Chemicals used for the experiments. 27

Table 3: Composition of the two different emulsions used for sensor preparation..... 30

Table 4: Protocol for sonication of the pH and O_2 cocktail. 32

Table 5: Parameters set for spotting the O_2 and pH sensor cocktails..... 33

Table 6: Parameter set for measuring fluorescent signal of CO_2, O_2 and pH sensor. 39

Table 7: Concentration range used for calibration and calculations to set correct values for mass flow controllers. 40

Table 8: pH values used for calibration at the two reaction temperatures. 41

Table 9: Composition of LB media for cultivation of *S. carnosus*. 42

Table 10: Composition of the LB-complex medium used for cultivation of *S. cerevisiae*..... 43

Table 11: Measured difference of the phase angles between 1.5 or 2 % and 5 % CO_2 in gas and liquid phase over time. 55

Tables and Figures

Table 12: Abbreviations used in this work..... 67

8 Appendix

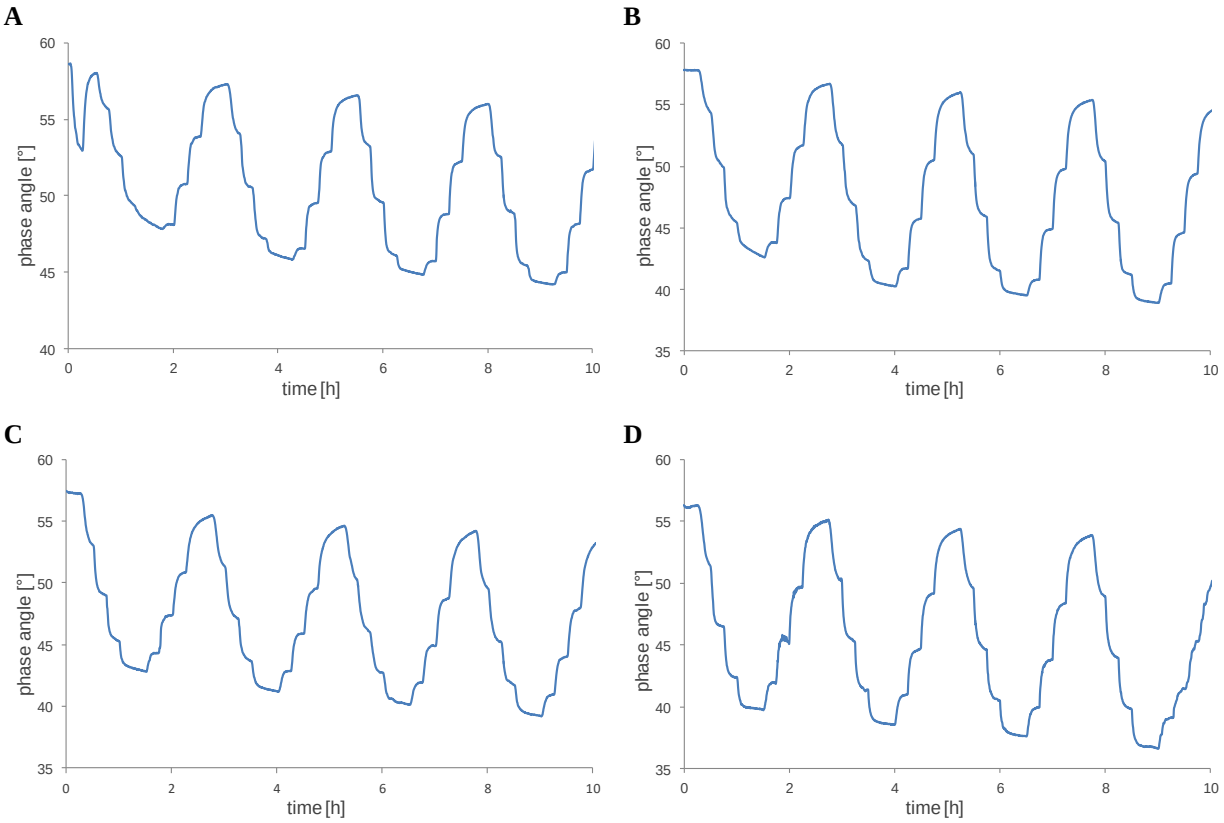

Figure 27: Comparison of the performance of the sensor foils: PDMS:D4 (10:1), 0.4 % monoOH, 10 % EB, dilution 2:1 (PDMS:HMS) and variations in film thickness and $CsHCO_3$ concentration. Measurement at 37 °C, in Tris-HCl buffer (0.1 M, pH 7.4). A: 250 mM $CsHCO_3$, 1 MIL, TiO_2; B: 150 mM $CsHCO_3$, 1 MIL, TiO_2; C: 250 mM $CsHCO_3$, 0.5 MIL, no TiO_2; D: 150 mM $CsHCO_3$, 0.5 MIL, no TiO_2.

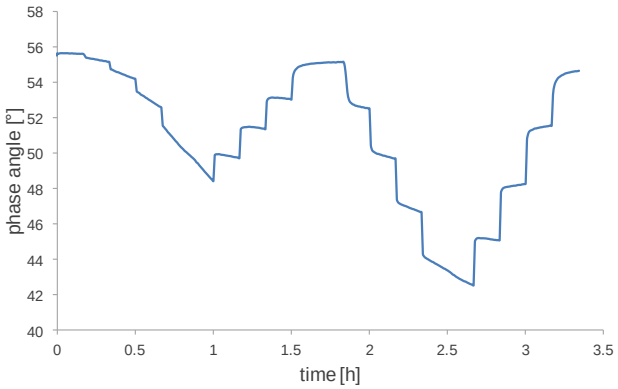

Figure 28: Measurement of sensorfoil PDMS:D4 (10:1) 0.4 % monoOH, 10 % EB, no dilution, 1 MIL, TiO_2 and $CsHCO_3$ (50 µL stock solution) in the gas phase.

Appendix

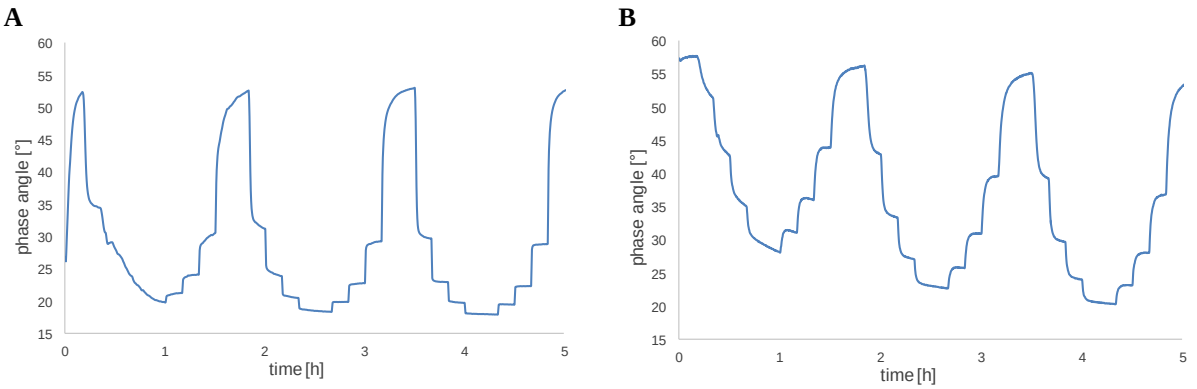

Figure 29: Comparison sensorfoils, PDMS:D4 (10:1), 250 mM $CsHCO_3$, 0.4 % monoOH, 10 % EB, 1 MIL, measured in ddH_2O at RT. A: diluted PDMS:HMS 2:1; B: undiluted.

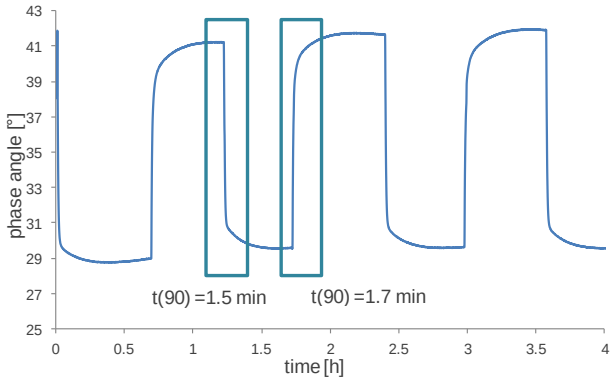

Figure 30: Response time measurement: Sensorfoil, PDMS:DMS (10:1), 250 mM $CsHCO_3$, 0.4 % monoOH, 10 % EB, 1 MIL, TiO_2, measured in Tris-buffer at RT.

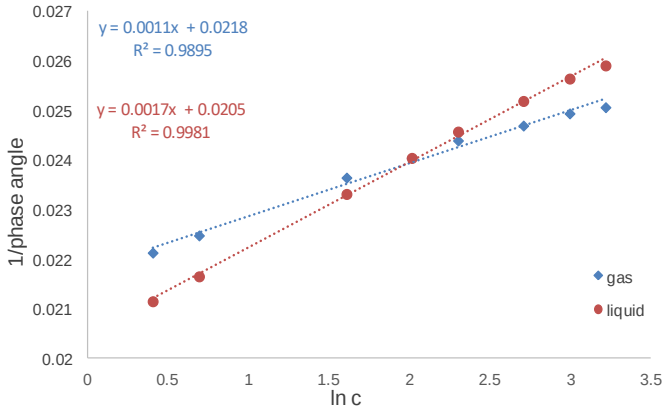

Figure 31: Example of a calibration for CO_2, between 1.5 and 25 % at 37 °C in KPi buffer or gas phase.

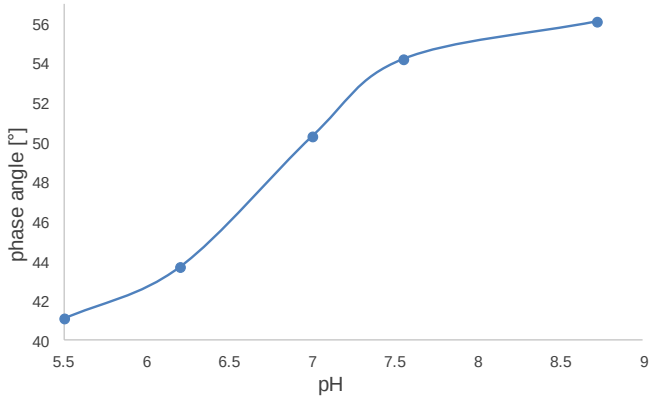

Figure 32: Example of a calibration for pH_2, between 5.5 and 8.7 at 37 °C in KPi buffer.